

## Responses to Referee #1

The manuscript studied the characteristics and changes of baseline ozone in oceanic air in East China based on 6-year continuous measurements conducted at an island site. Corresponding ozone changes under various transport conditions were detailed presented and the impacts of offshore ozone on ozone air quality in Shanghai were quantified using the WRF-Chem model. Since increasing ozone pollution has become an urgent environmental problem in coastal urban agglomerations in East China, the results of this study provide valuable insight into what needs to be considered in dealing with ozone pollution in coastal megacities like Shanghai.

We thank the reviewer for all the insightful comments. Please see our point-by-point response (in blue) to the general and specific comments below. The changes that have been made to the manuscript are also listed.

General comments: Results and discussion-Sect.3 presented the overall changes of ozone in oceanic air at SSI. However, the key point was not prominent enough in current version. I suggest focusing more on the novelties of the study (the changes of baseline  $O_3$  in oceanic air). Questions of why  $O_3$  changes in September and October were analyzed, and what could be the driver of the detected changes need to be deeply reformulated.

Response:

Thanks very much for pointing out that. We have rewritten Sect. 3.3 in the revised manuscript as suggested by the reviewer. Please see below:

“As discussed in Sect. 3.1, the prevailing winds carried different levels of pollutants to the SSI, resulting in different impacts on the  $O_3$  levels in different months. In September and October, the frequencies of SW and W winds that carried high levels of pollutants were lowest (Table 1–2), exerting least influence on the atmospheric composition at SSI. Therefore, the variations of surface  $O_3$  concentrations in September and October at SSI were examined to further assess the changes of least contaminated  $O_3$  in the oceanic air. Figure 6b presents the overall changes of daily mean surface  $O_3$  concentrations in

September and October at SSI and XJH, respectively during the six-year period. The corresponding mean O<sub>3</sub> mixing ratios during the two months were 60.9 and 31.3 ppbv, respectively at SSI and XJH. Compared to the significant elevated O<sub>3</sub> concentrations at XJH (0.59 ppbv yr<sup>-1</sup>,  $\alpha < 0.10$ ) in September and October, observed O<sub>3</sub> at SSI during same months exhibited insignificant decreasing changes from 2012–2017. The changes (-0.72 ppbv yr<sup>-1</sup>,  $\alpha > 0.10$ ) were somewhat different from the overall O<sub>3</sub> changes (+1.12 ppbv yr<sup>-1</sup>,  $\alpha > 0.10$ ) at SSI, suggesting different causes of the observed O<sub>3</sub> changes in the oceanic air during September and October.

To investigate possible drivers of the observed changes in the least contaminated O<sub>3</sub> in September and October at SSI, Table 3 displays the statistical results of the MK test and Theil-Sen trend estimate for NO<sub>x</sub> and CO mixing ratios, temperature, and wind speed during the 2012–2017 period. Statistically significant upward trends were detected in wind speed, with estimated increasing rates of 0.21 m s<sup>-1</sup> yr<sup>-1</sup> during the observation period ( $\alpha < 0.05$ ). The significantly enhanced surface wind speeds were conducive to the diffusion of O<sub>3</sub>, which might be an important meteorological driver of the observed decreasing changes in O<sub>3</sub> levels at SSI from 2012 to 2017. Observed NO<sub>x</sub> and CO levels exhibited increases of 0.48 ppbv yr<sup>-1</sup> ( $\alpha < 0.05$ ) and 2.67 ppbv yr<sup>-1</sup> ( $\alpha > 0.10$ ), respectively in September and October during the six-year period, indicating enhanced transport of pollutants to the oceanic area. Tie et al. (2013) suggested that the VOC-limited regime of O<sub>3</sub> formation was not only confined in urban Shanghai, but also extended to a broader regional area surrounding Shanghai. Thus, the elevated NO<sub>x</sub> concentrations might not only retard daytime O<sub>3</sub> production but also enhance nighttime O<sub>3</sub> depression at SSI. Figure 6c further presents corresponding variations of daytime (10:00-16:00 LST) and nighttime (23:00-04:00 LST) mean O<sub>3</sub> concentrations at SSI. Both daytime and nighttime O<sub>3</sub> concentrations exhibited downward changes, reflecting the O<sub>3</sub> response to the enhanced O<sub>3</sub> diffusion and depression in September and October. Therefore, the enhanced diffusion and depression of O<sub>3</sub> induced by the elevated wind speed and NO<sub>x</sub> concentrations might be important causes of the observed O<sub>3</sub> changes in September and October at SSI. It should be noted that the influence of radiation cannot be analyzed since

observations of solar radiation were not available during the study period. Therefore, more measurements are still needed to further understand the O<sub>3</sub> changes and corresponding drivers in the oceanic air.”

Specific comments:

1. Line 59: The location where the increased ozone concentrations were observed should be specified.

Response:

We have revised the sentence as “Based on 14-year observations at a coastal site in Hong Kong, Wang et al. (2009) pointed out that enhanced pollution flow from the upwind coastal regions contributed to most of the observed O<sub>3</sub> increases in the background atmosphere of South China during 1994–2007. And the increase in background O<sub>3</sub>, in turn, made a strong contribution of 81% to the increasing rate of O<sub>3</sub> in urban Hong Kong.”.

2. Line 69: Change “the three” to “those”

Response: Changed.

3. Line 73: Remove “surface”

Response: Removed.

4. Line 74: Change “atmospheric oxidation capacity response to” to “atmospheric oxidation capacity of continental air responding to”

Response: Changed.

5. Line 76: Change “in” to “at”

Response: Changed.

6. Line 91: Change “covering...area” to “covering an area of...”

Response: Changed.

7. Line 93: Change “magnitude” to “levels”

Response: Changed.

8. Line 120-121: Remove “In addition”

Response: Removed.

9. Line 125: Please explain the impact

Response:

This part has been revised as “The DT site was set up in a national nature reserve near the coast of Shanghai, where the observed pollutant levels have been reported to well reflect the impacts of megacities in the Yangtze River Delta (YRD) region on the remote atmosphere during the MIRAGE-Shanghai (Megacities Impact on Regional and Global Environment at Shanghai) field campaign”.

10. Line 158: Add “its” before “surrounding”

Response: Added.

11. Line 175: Change “require” to “requires”

Response: Changed.

12. Line 177: Add “to” before “be”

Response: Added.

13. Line 216: Change “cleaner” to “less polluted”

Response: Changed.

14. Line 228: Change “distinctions” to “variations”

Response: Changed.

15. Line 234: The observed O<sub>3</sub> at DT site need to be provided in the supplementary materials.

Response:

The mean diurnal variations of O<sub>3</sub> at DT during the period 2012–2017 have been added to the supplementary materials as Fig. S1. Please see below.

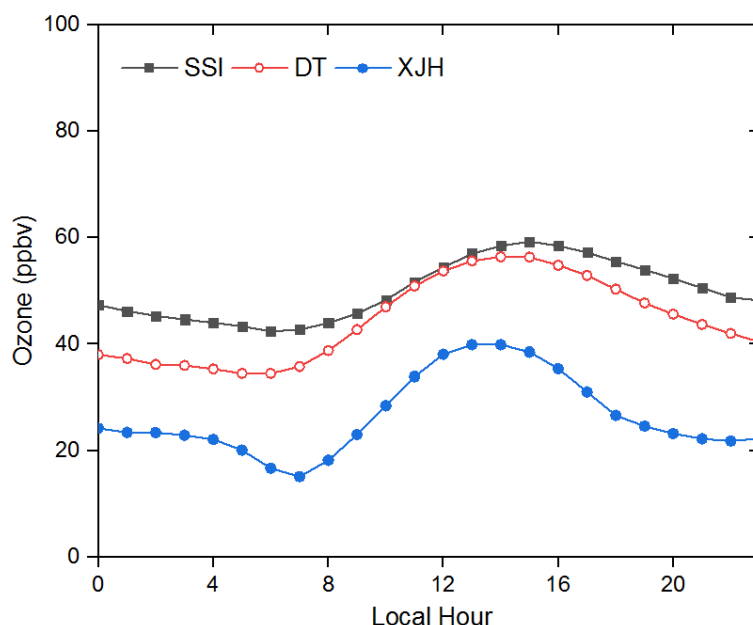


Fig. S1. Mean diurnal variations of O<sub>3</sub> at Sheshan Island (SSI, remote and oceanic), Dongtan (DT, rural), and Xujiahui (XJH, urban) station during the period 2012–2017.

16. Line 252: Actually, the study of Scheel et al. (1997) was conducted in Europe. Is 1.4 also a typical value of O<sub>3-max</sub>/O<sub>3-min</sub> in Chinese background sites? Please make sure of that.

Response:

Thanks for pointing out that. The following description has been added to the second paragraph of Sect. 3.2: "For regional background sites in China, the typical values of O<sub>3-max</sub>/O<sub>3-min</sub> were usually in the range of 2–3 (Xu et al., 2008; Meng et al., 2009; Gu et al., 2020). In Lin'an, a continental background site in YRD region, the ratio was reported to increase as a result of NO<sub>x</sub> emission changes during past decades, which could reach above 6 during summertime (Xu et al., 2008).".

17. Line 292: How about the trend of O<sub>3</sub> observed at DT and Lin'an?

Response:

Compared to those at SSI, observed extreme values of O<sub>3</sub> concentrations at DT and Lin'an were reported to exhibit more statistically significant ( $\alpha < 0.05$ ) changes response to the changes of anthropogenic emissions (e.g. NO<sub>x</sub>) in past decades (Xu et al., 2008; Gao et al., 2017; Gu et al., 2020). We have revised this part in the manuscript.

18. Line 298: Change “nearly uncontaminated” to “least contaminated”

Response: Changed.

19. Line 330: Change “variations of” to “changes in”

Response: Changed.

20. Line 396-397: Please specify the source of this conclusion. Reference or methods need to be added.

Response:

We have added Fig. S2 to the supplementary materials and revised this part as :  
According to the cluster analysis results (Fig. S2), easterly winds from the ocean greatly affected the Shanghai region, accounting for 64–78% of the total flows in non-winter months during the period 2012–2017.”

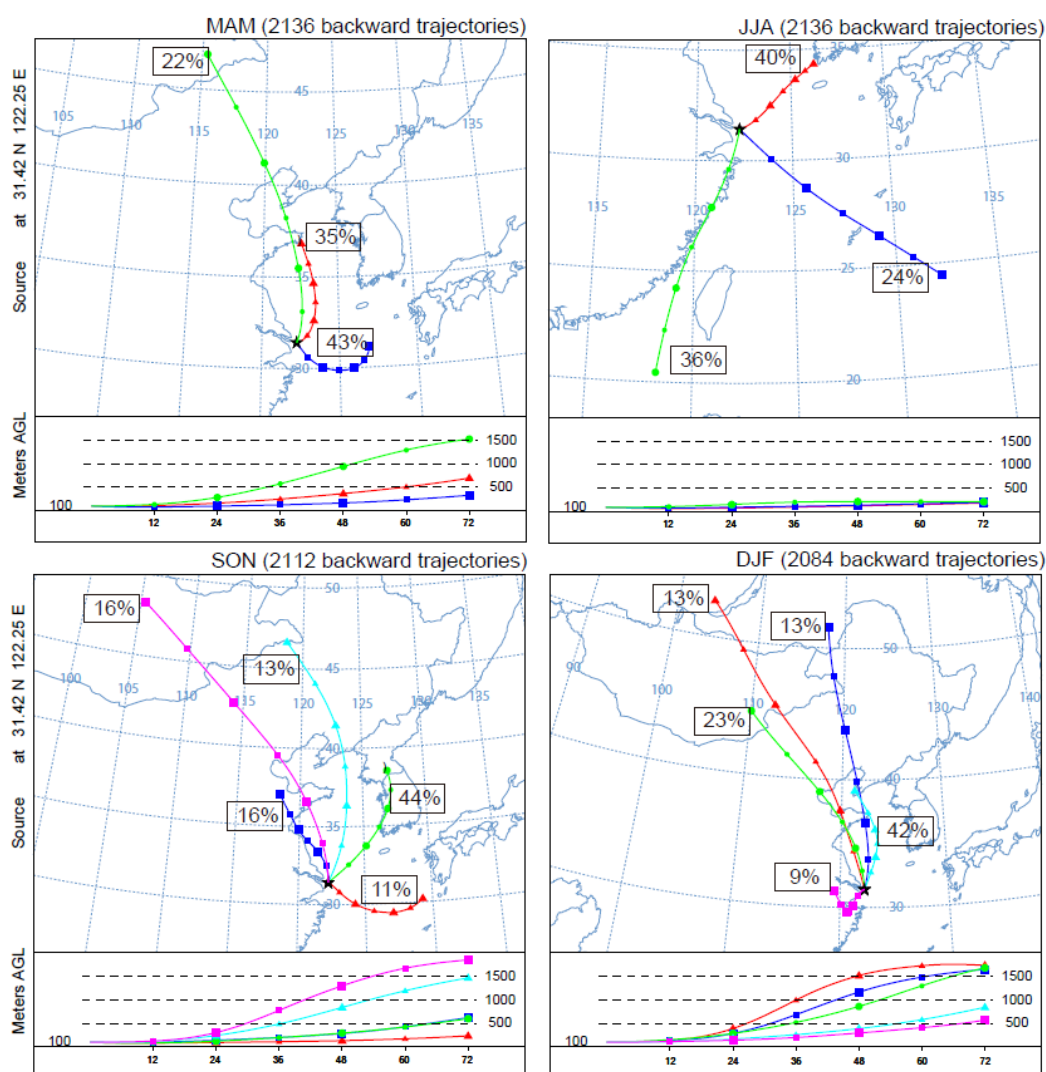


Fig. S2. Seasonal variations of the 72-h air mass backward trajectories arriving at the Sheshan Island (SSI) site using the Hybrid Single-Particle Lagrangian Integrated Trajectory (HYSPLIT) model (Version 4, Draxler and Hess, 1998) driven by NCEP/NCAR Global Reanalysis Data ( $2.5^{\circ} \times 2.5^{\circ}$ ). Trajectory clusters for MAM (March–May, left up), JJA (June–August, right up), SON (September–November, left bottom), and DJF (December–February, right bottom) were calculated based on the trajectories of 2012–2017 with steps of 12 h. The corresponding percentage occurrence values for different groups are presented as numbers in black squares.

21. Line 456: Do the 6-8 ppbv increases in  $O_3$  occur in downtown Shanghai? Please specify it.

Response:

This sentence has been revised as “Even so, simulated mean O<sub>3</sub> concentrations still exhibit 6–8 ppbv increases in downtown Shanghai in the BC<sub>60</sub> scenario, accounting for approximately 30% of the simulated O<sub>3</sub> concentrations in the BC<sub>40</sub> case.”.

22. Line 473: Change “mean concentrations” to “a mean value”

Response: Changed.

#### Reference

- Draxler, R. R. and Hess, G. D.: An overview of the HYSPLIT 4 modelling system for trajectories, dispersion, and deposition, *Austral. Meteorol. Mag.*, 47, 295–308, 1998.
- Gao, W., Tie, X., Xu, J., Huang, R., Mao, X., Zhou, G., and Chang, L.: Long-term trend of O<sub>3</sub> in a mega city (Shanghai), China: characteristics, causes, and interactions with precursors, *Sci. Total Environ.*, 603–604, 425–433, 2017.
- Gu, Y., Li, K., Xu, J., Liao, H., Zhou, G.: Observed dependence of surface ozone on increasing temperature in Shanghai, China. *Atmos. Environ.*, 221, 117108, 2020.
- Meng, Z. Y., Xu, X. B., Yan, P., Ding, G. A., Tang, J., Lin, W. L., Xu, X. D., and Wang, S. F.: Characteristics of trace gaseous pollutants at a regional background station in Northern China, *Atmos. Chem. Phys.*, 9, 927–936, <https://doi.org/10.5194/acp-9-927-2009>, 2009.
- Tie, X., Geng, F., Guenther, A., Cao, J., Greenberg, J., Zhang, R., Apel, E., Li, G., Weinheimer, A., Chen, J., and Cai, C.: Megacity impacts on regional ozone formation: observations and WRF-Chem modeling for the MIRAGE-Shanghai field campaign, *Atmos. Chem. Phys.*, 13, 5655–5669, 2013.
- Wang, T., Wei, X. L., Ding, A. J., Poon, C. N., Lam, Y. S., Li, Y. S., Chan, L. Y., and Anson, M.: Increasing surface ozone concentrations in the background atmosphere of Southern China, 1994–2007, *Atmos. Chem. Phys.*, 9, 6217–6227, 2009.
- Xu, X., Lin, W., Wang, T., Yan, P., Tang, J., Meng, Z., and Wang, Y.: Long-term trend of surface ozone at a regional background station in eastern China 1991–2006: enhanced variability, *Atmos. Chem. Phys.*, 8, 2595–2607, 2008.



## Responses to Referee #2

This study conducted observational and modeling analysis of baseline ozone in oceanic air at Sheshan Island (SSI), which is located to the east of Shanghai city. The authors reported a six-year measurement of ozone concentration at SSI and its ozone level is much higher than the value of downtown site in Shanghai. They further highlight the importance of understanding the interaction between urban plume and oceanic inflows in ozone pollution. In particular, their modeling results show that ozone in the oceanic inflows can enhance urban ozone by 20-30%.

We thank the reviewer for all the insightful comments. Please see our point-by-point response (in blue) to the general and specific comments below. The changes that have been made to the manuscript are also listed.

Overall, this manuscript is well structured and sits in the scope of this journal. Recent studies have increasingly focused on urban ozone pollution in China, but study on background ozone is still very limited. As such, this study could enrich our understanding of ozone pollution in China, particularly for coastal cities. Although this manuscript is publishable, the current version should be improved in terms of presentation and clarification. I would like the authors to address my following comments.

-This study shows observed ozone levels in a remote site and urban site. In fact, urban ozone in Shanghai are available from Chinese measurement network. It will be great if the authors could have more ozone measurements in this study. For example, Figure 8 is a good place to show more urban ozone data.

Response:

Thanks for the suggestions. Since  $O_3$  measurements in urban Shanghai from Chinese measurement network are only publicly available after March 2013, the data length cannot cover the whole study period in this study. To provide more measurements in Fig. 8, we added continuous  $O_3$  measurements obtained from Sheshan (SS), Pudong (PD), and DT (Dongtan) sites in Shanghai.  $O_3$  concentrations were measured using the

same method as those at SSI and XJH during the period 2012–2017. Figure 8 and Table 4 have been revised same as Fig. R1 and Table R1. Corresponding discussions in Sect. 3.5 are revised as follows:

“Figure 8 displays the simulated and observed monthly mean distributions of surface  $O_3$  concentrations in BC\_40, BC\_50 and BC\_60 scenarios, respectively. In addition to the observations at XJH and SSI,  $O_3$  measurements obtained from other three sites, Pudong (PD, suburban), Sheshan (SS, rural), and Dongtan (DT, rural), during the same period were introduced to evaluate the model's performance in simulating  $O_3$  in Shanghai. The  $O_3$  concentrations at all the sites were measured using the same method as described in Sect. 2.1. The calculated distributions of  $O_3$  agree with observations, which exhibit lower values in urban regions compared to those in rural and ocean areas, indicating strong  $O_3$  depressions in the city of Shanghai due to the VOC-limited  $O_3$  formation regime. The R values between the simulated and observed  $O_3$  concentrations are all larger than 0.50 at continental sites (XJH, PD, SS, and DT), suggesting good prediction of  $O_3$  variations by the model.

Table 4 displays the statistical results of the comparisons between the simulated and observed surface  $O_3$  concentrations at different sites in Shanghai. Generally, the WRF-Chem model underestimates  $O_3$  concentrations at all the sites in most cases. Taken the BC\_40 scenario for example, the  $O_3$  concentrations are underestimated by 9.4–27.6% at continental sites and 36.1% at SSI, suggesting larger underestimation of  $O_3$  concentrations in oceanic regions. Model results further suggest that elevated  $O_3$  levels in the eastern chemical BCs would lead to increases in  $O_3$  concentrations at both urban and remote sites when the prevailing winds are mostly easterly in Shanghai. With  $O_3$  concentrations increasing from 40 to 60 ppbv in the easterly oceanic air inflows, the simulated monthly mean  $O_3$  concentrations increase by 7.0–9.7 ppbv at continental sites and 10.4 ppbv at SSI. The underestimation of  $O_3$  levels by the model is also greatly improved in the BC\_60 scenario, when the chemical BCs of  $O_3$  are more close to the observations. Compared to those in the BC\_40 scenario, the normalized mean bias (NMBs) of the predicted  $O_3$  concentrations reduced at most sites in the BC\_60 scenario,

for example from -36.1 % to -18.1 % at SSI and -27.6% to -4.6% at XJH, suggesting a crucial role of the eastern oceanic air inflows in influencing O<sub>3</sub> air quality in Shanghai.”

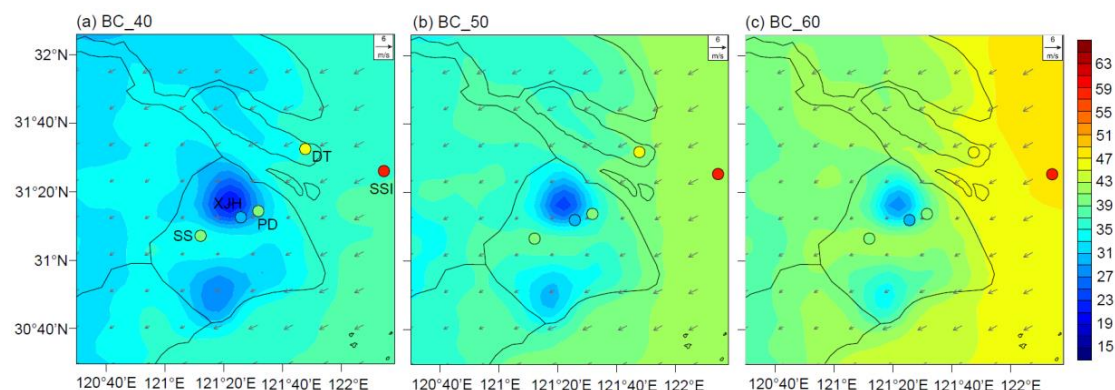


Figure R1 Calculated distributions of monthly mean O<sub>3</sub> concentrations (shades, ppbv) from BC\_40, BC\_50 and BC\_60 simulations, respectively in September 2014. Model results are compared with observed mean O<sub>3</sub> concentrations (circles, ppbv) obtained from Sheshan (SS), Xujiahua (XJH), Pudong (PD), DT (Dongtan) and Sheshan Island (SSI) sites. Also shown is the calculated wind field (m s<sup>-1</sup>) averaged over the same period.

Table R1 Statistical results of the comparisons between the simulated and observed surface O<sub>3</sub> concentrations at Sheshan (SS), Xujiahua (XJH), Pudong (PD), DT (Dongtan) and Sheshan Island (SSI) sites during September 2014. The calculated O<sub>3</sub> levels are obtained from BC\_40, BC\_50 and BC\_60 simulations, respectively. Values of the average surface O<sub>3</sub> concentrations (Mean) and normalized mean bias (NMB) are displayed. The NMB is defined as  $NMB = \frac{\sum_{i=1}^n (P_i - O_i)}{\sum_{i=1}^n O_i}$ , where  $P_i$  and  $O_i$  are predicted and observed ozone mixing ratios for sample  $i$ ,  $n$  is the number of total samples (numbers in parentheses).

	Cases	SS (681)	XJH (641)	PD (690)	DT (690)	SSI (720)
	Observation	39.7	30.4	40.3	46.4	57.7
Mean (ppbv)	BC_40	36.0	22.0	29.5	35.3	36.9
	BC_50	39.1	25.1	33.3	39.6	41.8
	BC_60	43.1	29.0	37.9	45.0	47.3
NMB(%)	BC_40	-9.4	-27.6	-26.7	-23.9	-36.1
	BC_50	-1.5	-17.5	-17.2	-14.5	-27.5

- This study gives daily mean of ozone in both observational and modeling calculation. I am wondering if the authors can show more results for MDA8 ozone. Since MDA8 ozone is the standard air quality metric for ozone.

Response:

Thanks for the suggestions. We have presented results for MDA8 O<sub>3</sub> in the revised manuscript. The new results added are as follows:

Sect. 3.2:” The observed mean daily maximum 8-h average (MAD8) O<sub>3</sub> concentrations exhibited same differences between the two sites, which were 40.1 and 62.0 ppbv, respectively at XJH and SSI.”

Sect. 3.3:” The monthly mean MDA8 and daily extreme values of O<sub>3</sub> exhibited similar differences between the two sites. The calculated increasing rates of MDA8 O<sub>3</sub>, O<sub>3-max</sub> and O<sub>3-min</sub> were 2.73, 2.77, and 1.35 ppbv yr<sup>-1</sup> ( $\alpha < 0.05$ ), respectively at XJH, and 1.01, 1.35, and 1.27 ppbv yr<sup>-1</sup> ( $\alpha > 0.10$ ), respectively at SSI.”

-Line 27: “production” might be more appropriate than “oxidation”.

Response: Revised.

-Line 89: please spell out months.

Response: Revised.

-Lines 252-253: will this ratio be helpful in this study?

Response:

The ratio of daily maximum O<sub>3</sub> concentration (O<sub>3-max</sub>) to minimum O<sub>3</sub> concentration (O<sub>3-min</sub>) was usually regarded as an indicator to identify if a site could be considered as a typical background site as suggested in previous studies (Cvitas and Klasinc 1993; Cvitas et al., 1995; Vingarzan, 2004). For SSI, the mean ratio of O<sub>3-max</sub>/O<sub>3-min</sub> was calculated to be 3.03 during the study period, which was consistent with the typical values observed at

continental background sites in China (Xu et al., 2008; Meng et al., 2009; Gu et al., 2020). In September and October, the ratio exhibited even low values at SSI, ranging from 1.61–2.35. The results helped to further indicate that the observed O<sub>3</sub> at SSI, especially in September and October, were least contaminated by regional pollution. And the SSI site could be regarded as a typical oceanic background site, providing a good proxy to study the baseline oxidation capacity of oceanic atmosphere in eastern China.

-Line 293: “few” looks not reasonable, since you still saw an increase trend of 1.12ppb yr<sup>-1</sup>.

Response:

Thanks for pointing out that. This part has been revised as :“... the statistically insignificant changes of O<sub>3</sub> detected at SSI indicated that O<sub>3</sub> in the oceanic air remained a constant level during the study period and was less influenced by the decreases of NO<sub>x</sub> emissions.”

-Lines 346-348: is there any changes in ozone production sensitivity in response to NO<sub>x</sub> control?

Response:

Yes. Based on measurements obtained from the same sites, Xu et al. (2019) has carefully examined the response of O<sub>3</sub> production sensitivity to NO<sub>x</sub> reductions in Shanghai during the past decade. The O<sub>3</sub> isopleth diagram (Fig. R2) constructed by the Ozone Isopleth Plotting Package Research (OZIPR) model suggested that the O<sub>3</sub> production had moved from strong VOC-limited regime to slight VOC-limited regime in both urban and suburban sites in Shanghai due to the significant NO<sub>x</sub> reductions and slight VOCs changes from 2009 to 2015. In 2017, the observed mean NO<sub>x</sub> concentrations at XJH and PD decreased by 3.5 and 0.3 ppbv, respectively compared to those (33.2 ppbv at XJH and 22.6 ppbv at PD) in 2015, indicating that the O<sub>3</sub> production could still be VOC-limited in Shanghai according to Fig. S1. The results suggested that the O<sub>3</sub> production remained VOC-limited in Shanghai during the study period and the changes in

O<sub>3</sub> production induced by NO<sub>x</sub> reductions did not affect the main conclusion of the manuscript.

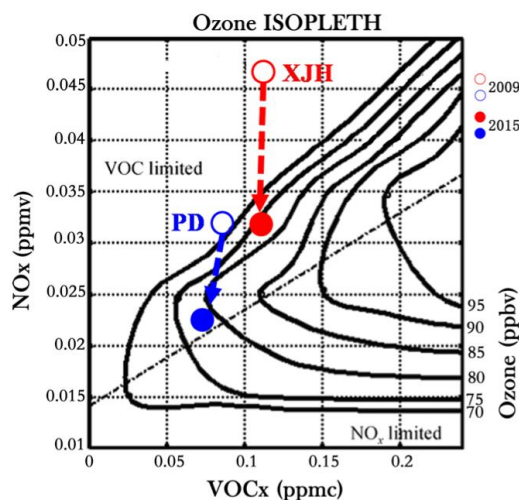


Figure R2 The O<sub>3</sub> isopleth diagram constructed by the OZIPR model in Shanghai (Xu et al., 2019).

We have revised this part as:” The results are in accordance with Tie et al. (2013) and Xu et al. (2019), who suggested that Shanghai and a broader regional area surrounding the city were all in the VOC-limited O<sub>3</sub> formation regime during the study period.”

-Line 397: remove space before “%”.

Response: Removed.

-Line 492:  $\alpha$  should be  $<0.05$  according to Table 3.

Response: Revised.

## Reference

- Cvitas, T., and Klasinc, L.: Measurement of tropospheric ozone in the Eastern Mediterranean, *Boll. Geofisico*, 16, 521–527, 1993.
- Cvitas, T., Kezele, N., Klasinc, L., and Lisac, J.: Tropospheric ozone measurements in Croatia, *Pure Appl. Chem.*, 67, 1450–1453, 1995.
- Gu, Y., Li, K., Xu, J., Liao, H., Zhou, G.: Observed dependence of surface ozone on increasing temperature in Shanghai, China. *Atmos. Environ.*, 221, 117108, 2020.
- Meng, Z. Y., Xu, X. B., Yan, P., Ding, G. A., Tang, J., Lin, W. L., Xu, X. D., and Wang, S. F.: Characteristics of trace gaseous pollutants at a regional background station in Northern China, *Atmos. Chem. Phys.*, 9, 927–936,

- <https://doi.org/10.5194/acp-9-927-2009>, 2009.
- Vingarzan, R.: A review of surface ozone background levels and trends, *Atmos. Environ.*, 38, 3431–3442, 2004.
- Xu, J., Tie, X., Gao, W., Lin, Y., and Fu, Q.: Measurement and model analyses of the ozone variation during 2006 to 2015 and its response to emission change in megacity Shanghai, China, *Atmos. Chem. Phys.*, 19, 9017–9035, 2019.
- Xu, X., Lin, W., Wang, T., Yan, P., Tang, J., Meng, Z., and Wang, Y.: Long-term trend of surface ozone at a regional background station in eastern China 1991–2006: enhanced variability, *Atmos. Chem. Phys.*, 8, 2595–2607, 2008.

1 **A measurement and model study on ozone characteristics in marine air at a remote**  
2 **island station and its interaction with urban ozone air quality in Shanghai, China**

3 Yixuan Gu<sup>a,b</sup>, Fengxia Yan<sup>c</sup>, Jianming Xu<sup>a,b,\*</sup>, Yuanhao Qu<sup>a,b</sup>, Wei Gao<sup>a,b</sup>

4 <sup>a</sup>Shanghai Typhoon Institute, Shanghai Meteorological Service, Shanghai 200030, China

5 <sup>b</sup>Shanghai Key Laboratory of Meteorology and Health, Shanghai Meteorological Service,  
6 Shanghai 200030, China

7 <sup>c</sup>Meteorological Center of Traffic Management of East China, Shanghai 2000135, China

8 Corresponding to: Dr. Jianming Xu ([metxujm@163.com](mailto:metxujm@163.com))

9

10 **Keywords:** Ozone in oceanic air, Urban Plume, Coastal city air pollution, Shanghai



## Abstract

To understand the characteristics and changes of baseline ozone ( $O_3$ ) in oceanic air in East China, a six-year measurement of  $O_3$  concentration was conducted from January 1 2012 to September 15 2017 at a remote offshore station located on the Sheshan Island (SSI) near the megacity of Shanghai. The observed monthly mean  $O_3$  concentrations at SSI ranged from 33.4 to 61.4 ppbv during the study period, which were about 80% and 12% higher, respectively than those measured at downtown and rural sites in Shanghai. Compared to the remarkable  $O_3$  increases observed at urban and rural sites in Shanghai, observed  $O_3$  concentrations at SSI exhibited statistically insignificant increasing changes ( $1.12 \text{ ppbv yr}^{-1}$ ,  $\alpha > 0.10$ ) during the observation period, suggesting less impacts of anthropogenic emissions on  $O_3$  levels in oceanic air. In addition, an insignificant decreasing change ( $-0.72 \text{ ppbv yr}^{-1}$ ,  $\alpha > 0.10$ ) was detected in  $O_3$  concentrations at SSI in September and October when the influence of regional transport was minimum throughout the year, providing a good proxy to study the baseline oxidation capacity of the oceanic atmosphere. City plumes from Shanghai usually carried higher levels of  $NO_x$ , resulting in decreased  $O_3$  concentrations at SSI during southwesterly and westerly winds. However, In MAM (March–May) and JJA (June–August), due to the enhanced production of oxygenated volatile organic compounds,  $O_3$  could be continuously produced during daytime in aged city plumes, resulting in elevated  $O_3$  concentrations transported to SSI. The impacts of the offshore  $O_3$  on  $O_3$  levels in Shanghai are quantified during an easterly wind dominant episode (September 1–30, 2014) using the WRF-Chem model. Sensitivity results suggest that  $O_3$  in the oceanic air inflows can lead to 20–30% increases in urban

- 33  $\text{O}_3$  concentrations, which should be crucially considered in dealing with urban  $\text{O}_3$  pollution
- 34 in large coastal cities like Shanghai.

## 1 Introduction

Ground-level ozone ( $O_3$ ) is a harmful photochemical oxidant detrimental to air quality, human health and land ecosystems (Yue and Unger 2014; Monks et al., 2015; Li et al., 2019a). High ambient  $O_3$  has been proved to increase the risks of respiratory and cardiovascular mortality (Goodman et al., 2015) and enhance the greenhouse effect (IPCC, 2013). In recent years,  $O_3$  pollution has drawn increasing attention in China, since  $O_3$  pollution is getting worse in spite of the implementation of Chinese Clean Air Action Plan. In contrast to the 28-40% decreases in  $PM_{2.5}$  (fine particulate matter; diameter  $\leq 2.5$   $\mu m$ ) levels, the observed daily maximum 8-h average (MDA8)  $O_3$  concentrations show increasing rates of 1–3 ppb  $yr^{-1}$  in summer in megacities over eastern China during 2013–2017 (Li et al., 2019b). To address the underlying causes of the increasing  $O_3$  pollution has become an urgent issue that triggers lots of discussions based on observational and model studies worldwide (Yang et al., 2014; Lou et al., 2015; Fu et al., 2019).

Observational and model studies indicated that the elevated  $O_3$  levels in urban and rural areas in eastern China were strongly related to the changes in anthropogenic emissions of  $O_3$  precursors (Ma et al., 2016; Lu et al., 2018; Li et al., 2019b; Gu et al., 2020). Since the  $O_3$  formation was reported to be under volatile organic compound (VOC) limited regime in most Chinese megacities (e.g. Beijing, Shanghai, and Guangzhou), the sharp decreases in nitrogen oxides ( $NO_x=NO+NO_2$ ) emissions combined with slight increases in VOC levels were suggested to be main causes of the observed enhancement of  $O_3$  concentrations in East China (Gao et al., 2017; Xu et al., 2019). In remote areas, changes of baseline  $O_3$  also exhibit sensitive responses to human activities (Vingarzan,

2004; Meng et al., 2009; Wang et al., 2009; Lin et al., 2015). Based on 14-year observations at a coastal site in Hong Kong, Wang et al. (2009) pointed out that enhanced pollution flow from the upwind coastal regions contributed to most of the observed O<sub>3</sub> increases in the background atmosphere of South China during 1994–2007. And the increase in background O<sub>3</sub>, in turn, made a strong contribution of 81% to the increasing rate of O<sub>3</sub> in urban Hong Kong. It is thus necessary to understand the background O<sub>3</sub> changes and their responses to different sources when developing long-term strategies to mitigate local O<sub>3</sub> pollution. However, compared to the intensive field studies in polluted cities and surrounding rural regions, continuous observations of O<sub>3</sub> at representative background sites in China are relatively limited (Wang et al., 2017).

To better understand the characteristics of the background O<sub>3</sub> changes in mainland China, the China Meteorological Administration (CMA) started to conduct continuous measurements of surface O<sub>3</sub> at several regional background stations (e.g. Shangdianzi, Linan, and Longfengshan) since 2005. Over 10-year records from those sites and Waliguan, a baseline Global Atmospheric Watch (GAW) station in Tibetan Plateau region, exhibited different increases in background continental O<sub>3</sub> concentrations especially during daytime in China (Lin et al., 2008; Xu et al., 2008; Meng et al., 2009; Ma et al., 2016; Xu et al., 2016). The detected positive trends of O<sub>3</sub> were in a range of 0.24–1.13 ppbv yr<sup>-1</sup>, suggesting enhanced atmospheric oxidation capacity of continental air responding to the rapid development of urbanization and industrialization in the past decades. In addition to the changes at background O<sub>3</sub> in terrestrial stations mentioned above, the characteristics of baseline O<sub>3</sub> at remote marine sites are also important. It is

because that large amounts of O<sub>3</sub> pollution events occurred in coastal urban agglomerations in East China (Lu et al., 2018; Li et al., 2019a, b), affected by both city plumes and oceanic air inflows (Tie et al., 2009; Shan et al., 2016). For example, model work of Tie et al. (2009) suggested that sea air masses carried by oceanic inshore air flows aggravated urban O<sub>3</sub> pollution in Shanghai under convergence conditions. Understanding the O<sub>3</sub> characteristics in offshore oceanic regions is therefore an important prerequisite for understanding the land-sea O<sub>3</sub> interactions and its impacts on O<sub>3</sub> pollution in coastal cities. However, to our knowledge, studies on the characteristics and changes of O<sub>3</sub> in marine air are quite limited in mainland China since it is very difficult to conduct systematic and continuous observations under remote oceanic air conditions.

In this report, we present the first relatively long and continuous measurements of O<sub>3</sub> conducted on a remote offshore island (Sheshan Island, SSI) from [January 2012 to September 2017](#) in eastern China. The SSI is located at the confluence of the Yellow Sea and the East China Sea, [covering an area of about 0.4 km<sup>2</sup>](#). Since there are no inhabitants in the island, the observed O<sub>3</sub> is seldom affected by local anthropogenic emissions. The collected O<sub>3</sub> data are used to understand the [levels](#) and variabilities of O<sub>3</sub> in the offshore regions and their impacts on the O<sub>3</sub> concentrations in coastal city areas. First shown are the general impacts of regional transport on the remote atmosphere over the SSI region. Then the diurnal patterns of O<sub>3</sub> at SSI are investigated by comparing them with those observed at a downtown site (XJH) in Shanghai. Multi-year changes of O<sub>3</sub> concentrations at SSI are analyzed to examine the overall changes of baseline O<sub>3</sub> in marine air and possible causes. Also analyzed are the impacts of urban plumes on O<sub>3</sub> levels in oceanic

air in offshore regions. At last, the influence of  $O_3$  carried by oceanic air inflows on urban  $O_3$  air quality in Shanghai is assessed using the Weather Research and Forecasting model coupled with Chemistry (WRF-Chem).

## 2 Material and methods

### 2.1 The SSI site and ozone observations

To investigate the characteristics and variabilities of  $O_3$  in marine air and their interactions with urban air quality in coastal areas, ground  $O_3$  concentrations were continuously measured at SSI site ( $31.4^\circ N$ ,  $122.3^\circ E$ , 73.5 m a.s.l.), which is approximately 75 kilometers away from the east edge of Shanghai city. Figure 1 shows the location of SSI and the surrounding environment. As mentioned in Sect. 1, there is no resident and tourist on the island. The observed  $O_3$  at SSI site can represent the background  $O_3$  conditions in oceanic air which are seldom contaminated by anthropogenic emissions. Hourly  $O_3$  data was collected during January 1 2012 to September 15 2017, with a capture rate of 89.7%.  $O_3$  was measured using an analyzer from Ecotech, Australia (Model EC9810), which combined microprocessor control with ultraviolet photometry. The instrument met the technical specifications for United States Environmental Protection Agency, with a quality control check every 3 days, filter replaced every 2 weeks and calibration every month.

### 2.2 Observational data at urban and rural sites in Shanghai

To better understand the characteristics of the offshore  $O_3$  in oceanic air at SSI,  $O_3$  observations obtained from a downtown site, Xujiahui (XJH) are used for comparisons. The XJH site is located at downtown Shanghai, approximately 80 km west from the SSI. Since measurements of  $NO_x$ , carbon monoxide (CO) and meteorological parameters (e.g.

wind direction and wind speed) were unavailable at SSI, observations obtained at an adjacent site, Dongtan (DT), are substituted for the investigation. The DT site was set up in a national nature reserve near the coast of Shanghai, where the observed pollutant levels have been reported to well reflect the impacts of megacities in the Yangtze River Delta (YRD) region on the remote atmosphere during the MIRAGE-Shanghai (Megacities Impact on Regional and Global Environment at Shanghai) field campaign (Tie et al., 2013). Similar to SSI, the DT site is also little affected by human activities. The obtained observations of meteorology and pollutants are therefore applied for analyzing the impacts of regional transport on observed O<sub>3</sub> concentrations at SSI. NO<sub>x</sub> concentrations were measured with a chemiluminescent trace level analyzer (TEI; Model 42iTL), with detection limit of 0.025 ppb. CO concentrations were measured by the Model 48iTL Enhanced CO analyzer, based on gas filter correlation technology. The wind speed and wind direction were measured by using a DZZ4 Automatic Weather Station certificated by the China Meteorological Administration. The geographical locations and surrounding environment of XJH, DT, and SSI are displayed in Fig. 1.

### 2.3 The WRF-Chem model

We simulate O<sub>3</sub> using the regional chemical transport model WRF-Chem (version 3.8, <https://www2.aom.ucar.edu/wrf-chem>), collaboratively developed through efforts of several institutes, such as the National Center for Atmospheric Research (NCAR) and the National Oceanic and Atmospheric Administration (the National Centers for Environmental Prediction (NCEP)). The model includes on-line calculation of meteorological parameters, transport, mixing, emission, and chemical transformation of trace gases and aerosols

(Grell et al., 2005). The Regional Acid Deposition Model version 2 (RADM2, Stockwell et al., 1990) gas-phase chemical mechanism is used for the O<sub>3</sub> formation chemistry. Photolysis rates are calculated by using the fast radiation transfer module (FTUV) followed those in Madronich and Flocke (1999) and Tie et al. (2003). ISORROPIA II secondary inorganic (Fountoukis and Nenes, 2007) and the Secondary ORGANic Aerosol Model (SORGAM) (Schell et al., 2001) schemes are used for aerosol chemistry. Dry deposition follows the standard resistance-in-series model of Wesely (1989). The major physical processes employed in the model follow the Lin microphysics scheme (Lin et al., 1983), the Yonsei University (YSU) planetary boundary layer (PBL) scheme (Hong and Lim, 2006), the Noah Land surface model (Chen and Dudhia, 2001), and the long-wave radiation parameterization (Dudhia, 1989).

The model used in this study has a horizontal resolution of 6km×6km, including 150 un-staggered grids in west-east, 150 un-staggered grids in south-north, and 35 vertical layers extending from the surface to 50 hPa. The domain encompasses Shanghai and its surrounding region, centered at 31.3°N, 121.4°E. The NCEP FNL (Final) Operational Global Analysis data are used for meteorological initial and boundary conditions, with lateral meteorological boundary updated every 6 h. Basic chemical lateral boundary conditions are constrained by a global chemical transport model (MOZART-4, Model for OZone And Related chemical Tracers, version 4) (Tie et al., 2001; Emmons et al., 2010). Anthropogenic emissions are derived from the Multi-resolution Emission Inventory for China (MEIC inventory, <http://www.meicmodel.org/>; Li et al., 2014) for year 2010. Biogenic emissions are calculated online using model of emissions of gases and aerosols from



nature (MEGAN2, Guenther et al., 2006).

## 2.4 Methods for assessing the trend of ozone

The daily mean  $O_3$  concentrations are used to examine the overall changes in  $O_3$  concentrations during the period 2012–2017, including all time of day with qualified measurements. The trends are assessed using two nonparametric methods, which are commonly used to detect trends of non-normally distributed data with seasonality (Xu et al., 2016). The Mann-Kendall (MK) trend test (Mann, 1945; Kendall, 1975; Gilbert, 1987) is used to examine the trend significance, and the Theil-Sen trend estimate method (Sen, 1968) is used to estimate the slope of trend, which could also be considered as the rate of change, during the six-year period. Compared to the linear fitting analysis which requires data to be independent and follow a Gaussian distribution, the non-parametric trend test methods only need the data to be independent (Gocic and Trajkovic, 2013). To determine if the calculated rate of change is statistically significant, the confidence level of at least 95% is adopted in the MK trend test, with  $\alpha$  value less than 0.05 being considered a statistically significant trend. The trend significance is examined by comparing the value of a standardized test statistic  $Z$  to that of a standard normal variate at a given significance level ( $Z_\alpha$ ,  $\alpha=0.05$ ). If  $|Z| > Z_{1-\alpha/2}$ , then the dataset is non-stationary, exhibiting either an increasing or a declining trend; If  $|Z| \leq Z_{1-\alpha/2}$ , then the dataset is stationary with no significant trend. Detailed calculation of  $Z$  can be referred to Xu et al. (2016).

## 3 Results and discussion

### 3.1 Regional transport characteristics at SSI

The observed  $O_3$  concentrations at SSI were inevitably influenced by regional transport

189 depending on the prevailing winds in various seasons. Figure 2 displays the monthly wind  
190 rose diagrams averaged over the period of 2012 to 2017 at DT. As mentioned in Sect. 2.2,  
191 the DT site is a rural site located quite close to SSI. The observed wind speeds and wind  
192 directions could then be applied to deduce the origins of the air mass arriving at SSI in  
193 adjacent region. Generally, observed prevailing winds exhibited distinct seasonal  
194 variabilities which were greatly affected by the East Asian monsoon. In warm seasons  
195 (May-August), the site was predominately influenced by easterly and southeasterly winds,  
196 accounting for 40–50% of the total winds. While in cold seasons (November-February),  
197 the northwesterly and northerly winds became the predominant flows that affected SSI,  
198 accounting for about 45% of total winds. During transitional months (e.g. March, April,  
199 September and October), the dominant winds presented more diversities, with wind  
200 directions dispersedly distributed in all the directions. The observed seasonal variations of  
201 prevailing winds are typical at coastal cities at mid-latitude region (Shan et al., 2016; Xu et  
202 al., 2019), suggesting that air masses arriving at SSI originated from various regions and  
203 could result in different impacts on the offshore atmospheric composition in different  
204 months.

205 Since CO has a relative long chemical lifetime of a few months, the observed CO  
206 concentrations at DT could be regarded as a consequence of regional transport from  
207 polluted regions (Tie et al., 2009). Figure 3 displays the observed monthly mean CO  
208 mixing ratios under wind directions of north (N), northeast (NE), east (E), southeast (SE),  
209 south (S), southwest (SW), west (W), and northwest (NW) at DT during the 2012–2017  
210 period. Observed CO exhibited relative higher concentrations under SW and W winds in

all months, with mean mixing ratios of 0.44 and 0.56 ppmv, respectively during 2012–2017 (Table 1). The observed high CO mixing ratios suggested that the atmosphere constituents at SSI could be more affected by regional transport of air pollutants under SW and W wind conditions. As SSI is located to the northeast of the Shanghai city (Fig. 1), air masses carried by the SW and W flows usually contain more urban pollutants from upwind city areas, and those carried by E, SE, and NE flows mostly come from the ocean. The oceanic air masses are less polluted compared to those from the cities, leading to lower CO mixing ratio at SSI. For example, observed CO exhibited a mean concentration of 0.23 ppmv under SE wind conditions, which was about 50% lower than that influenced by W winds. To further examine the impacts of the SW and W winds on the atmosphere constituents at SSI, Table 2 lists the calculated monthly mean occurrence frequency of the SW and W winds in separate months during the studied period. The SW and S winds were most infrequent in September (6.1 %) and October (5.2 %), suggesting that the atmosphere at SSI during the two months could be less contaminated by pollutants transported from the city and might be more close to the baseline oceanic air conditions.

### 3.2 The diurnal pattern of ozone at SSI

Figure 4 displays the monthly mean diurnal variations of  $O_3$  at SSI and XJH in different months during 2012–2017. The observed  $O_3$  concentrations at the two sites exhibited similar seasonal variations, with monthly mean values highest (61.4 ppbv for SSI and 35.9 ppbv for XJH) in May and lowest (33.4 ppbv for SSI and 12.5 ppbv for XJH) in December. Since the  $O_3$  formation in urban Shanghai is VOC-limited, observed  $O_3$  could be significantly depressed by large  $NO_x$  emissions at downtown site (XJH) (Gu et al., 2020).

In Fig. 4, observed O<sub>3</sub> levels at XJH were quite lower than those at SSI in all months, with mean concentrations of 27.8 and 50.1 ppbv, respectively at XJH and SSI during the observation period. The observed mean daily maximum 8-h average (MAD8) O<sub>3</sub> concentrations exhibited same differences between the two sites, which were 40.1 and 62.0 ppbv, respectively at XJH and SSI. The observed mean O<sub>3</sub> concentration at SSI was also higher than that at DT (44.7 ppbv, Fig. S1) which is more close to the city, suggesting that O<sub>3</sub> levels in marine air could be higher than those at continental urban and rural sites. The observed diurnal patterns of O<sub>3</sub> at SSI and XJH in Fig. 4 were similar to those reported for other sites in eastern China (Xu et al., 2008; Geng et al., 2015; Gao et al., 2017), exhibiting minimums in early morning (06:00–08:00 LST) and maximums in the afternoon (13:00–15:00 LST). However, compared to those at the urban site (XJH), observed amplitudes of O<sub>3</sub> diurnal variations were much smaller at SSI. The diurnal variations of surface O<sub>3</sub> can be mainly attributed to the O<sub>3</sub> production through photochemical reactions in the daytime and O<sub>3</sub> depression via NO titration at nighttime (Sillman, 2003). Due to few emissions of O<sub>3</sub> precursors (NO<sub>x</sub> and VOCs), the O<sub>3</sub> production and depression could be weaker at remote site, resulting in flatter diurnal cycle of O<sub>3</sub> compared to that at polluted urban site.

Since the amplitudes of O<sub>3</sub> diurnal variations usually exhibited much smaller values in background areas compared to those in polluted urban regions, the ratio of daily maximum O<sub>3</sub> concentration (O<sub>3-max</sub>) to minimum O<sub>3</sub> concentration (O<sub>3-min</sub>) was regarded as an indicator to identify if the local O<sub>3</sub> pollution was significantly influenced by anthropogenic emissions (Cvitas and Klasinc 1993; Vingarzan, 2004). The O<sub>3-max</sub>/O<sub>3-min</sub>

ratio displayed larger values in polluted regions (Cvitas et al., 1995) and lower values in less contaminated rural regions. A ratio of about 1.4 suggested that the site could be regarded as a typical background site (Scheel et al., 1997). For regional background sites in China, the typical values of  $O_{3-max}/O_{3-min}$  were usually in the range of 2–3 (Xu et al., 2008; Meng et al., 2009; Gu et al., 2020). In Lin'an, a continental background site in YRD region, the ratio was reported to increase as a result of  $NO_x$  emission changes during past decades, which could reach above 6 during summertime (Xu et al., 2008). In Fig. 4, observed  $O_3$  displayed different diurnal variabilities in various months at SSI. The variations of the  $O_{3-max}/O_{3-min}$  ratio suggested different influence of regional transport on  $O_3$  levels in the marine atmosphere.

Figure 5 displays the calculated monthly mean  $O_{3-max}/O_{3-min}$  ratios at SSI and XJH, respectively during 2012–2017. Generally, the observed ratios of  $O_{3-max}/O_{3-min}$  at SSI were much lower than those at XJH in all the months, suggesting less impact of anthropogenic emissions on  $O_3$  levels. The calculated mean ratios were 3.03 and 5.20, respectively at SSI and XJH, and most of the calculated values were larger than 4.50 at the urban site. Besides, the ratios presented distinct seasonal differences at XJH and SSI sites. Higher values were observed in summer, indicating stronger photochemical production of daytime  $O_3$  during June to August. At SSI, the  $O_{3-max}/O_{3-min}$  ratio exhibited relatively low values in September and October, ranging from 1.61–2.35 during the studied period. The values were consistent with the typical values of  $O_{3-max}/O_{3-min}$  observed at continental background sites in China (Xu et al., 2008; Meng et al., 2009; Gu et al., 2020). Since the observed temperature and solar radiation still exhibited higher values during the two

months in Shanghai (Gao et al., 2017), the observed low O<sub>3</sub> diurnal amplitudes should not be attributed to the weakened photochemical formation of O<sub>3</sub> as those in winter. Due to the persistent control of anticyclone, Shanghai and its neighboring areas are usually dominated by stable weather conditions in September and October, resulting in more gentle and diversified wind conditions. During the two months, the occurrences of more polluted SW and W winds were lowest (6.1% and 5.2%) throughout the year. The corresponding wind speed (2.49 and 2.50 m s<sup>-1</sup>) also exhibited values 20% lower than those in other months (Table 2). The transport conditions led to fewer pollutants transported to the SSI region, which could explain the observed weak diurnal variabilities of O<sub>3</sub> in September and October. The transport conditions together with O<sub>3</sub> response further confirmed that the transport of city pollutants had minimum impacts on the offshore O<sub>3</sub> levels in oceanic air at SSI in September and October, providing a good proxy to study the baseline oceanic O<sub>3</sub> and oxidation capacity of background atmosphere in eastern China.

### 3.3 Overall changes of ozone in oceanic air at SSI

Several studies have observed increasing trends of ground-level O<sub>3</sub> in metropolitan areas over eastern China since 2013, suggesting that the O<sub>3</sub> increases were mostly attributed to the NO<sub>x</sub> emission reductions (Ma et al., 2016; Gao et al., 2017; Lu et al., 2018; Li et al., 2019b). However, the O<sub>3</sub> changes at remote sites were relatively not well elucidated during past years. Figure 6a presents the monthly variations of O<sub>3</sub> concentrations at SSI and XJH during the 2012–2017 period. The statistical results of the MK test and Theil–Sen trend estimate method indicated that observed monthly mean O<sub>3</sub> mixing ratios (O<sub>3-ave</sub>) exhibited increasing changes at both urban (XJH) and remote sites (SSI) in Shanghai,

with calculated increasing rate of 1.97 and 1.12 ppbv yr<sup>-1</sup>, respectively in XJH and SSI. Though an overall upward trend of O<sub>3</sub> was detected at SSI, the changes were not as remarkable as those observed at XJH, which could not even pass the MK trend test at the 90% confidence level. The monthly mean MDA8 and daily extreme values of O<sub>3</sub> exhibited similar differences between the two sites. The calculated increasing rates of MDA8 O<sub>3</sub>, O<sub>3-max</sub> and O<sub>3-min</sub> were 2.73, 2.77, and 1.35 ppbv yr<sup>-1</sup> ( $\alpha < 0.05$ ), respectively at XJH, and 1.01, 1.35, and 1.27 ppbv yr<sup>-1</sup> ( $\alpha > 0.10$ ), respectively at SSI. Compared to the rapid O<sub>3</sub> increases in urban Shanghai which was suggested to mostly result from the significant NO<sub>x</sub> emission reductions in the past decade (Gao et al., 2017; Xu et al., 2019), the statistically insignificant changes of O<sub>3</sub> detected at SSI indicated that O<sub>3</sub> in the oceanic air remained a relative constant level during the study period and was less influenced by the decreases of NO<sub>x</sub> emissions.

As discussed in Sect. 3.1, the prevailing winds carried different levels of pollutants to the SSI, resulting in different impacts on the O<sub>3</sub> levels in different months. In September and October, the frequencies of SW and W winds that carried high levels of pollutants were lowest (Table 1–2), exerting least influence on the atmospheric composition at SSI. Therefore, the variations of surface O<sub>3</sub> concentrations in September and October at SSI were examined to further assess the changes of least contaminated O<sub>3</sub> in the oceanic air. Figure 6b presents the overall changes of daily mean surface O<sub>3</sub> concentrations in September and October at SSI and XJH, respectively during the six-year period. The corresponding mean O<sub>3</sub> mixing ratios during the two months were 60.9 and 31.3 ppbv, respectively at SSI and XJH. Compared to the significant elevated O<sub>3</sub> concentrations at

XJH ( $0.59 \text{ ppbv yr}^{-1}$ ,  $\alpha < 0.10$ ) in September and October, observed  $\text{O}_3$  at SSI during same months exhibited insignificant decreasing changes from 2012–2017. The changes ( $-0.72 \text{ ppbv yr}^{-1}$ ,  $\alpha > 0.10$ ) were somewhat different from the overall  $\text{O}_3$  changes ( $+1.12 \text{ ppbv yr}^{-1}$ ,  $\alpha > 0.10$ ) at SSI, suggesting different causes of the observed  $\text{O}_3$  changes in the oceanic air during September and October.

To investigate possible drivers of the observed changes in the least contaminated  $\text{O}_3$  in September and October at SSI, Table 3 displays the statistical results of the MK test and Theil-Sen trend estimate for  $\text{NO}_x$  and CO mixing ratios, temperature, and wind speed during the 2012–2017 period. Statistically significant upward trends were detected in wind speed, with estimated increasing rates of  $0.21 \text{ m s}^{-1} \text{ yr}^{-1}$  during the observation period ( $\alpha < 0.05$ ). The significantly enhanced surface wind speeds were conducive to the diffusion of  $\text{O}_3$ , which might be an important meteorological driver of the observed decreasing changes in  $\text{O}_3$  levels at SSI from 2012 to 2017. Observed  $\text{NO}_x$  and CO levels exhibited increases of  $0.48 \text{ ppbv yr}^{-1}$  ( $\alpha < 0.05$ ) and  $2.67 \text{ ppbv yr}^{-1}$  ( $\alpha > 0.10$ ), respectively in September and October during the six-year period, indicating enhanced transport of pollutants to the oceanic area. Tie et al. (2013) suggested that the VOC-limited regime of  $\text{O}_3$  formation was not only confined in urban Shanghai, but also extended to a broader regional area surrounding Shanghai. Thus, the elevated  $\text{NO}_x$  concentrations might not only retard daytime  $\text{O}_3$  production but also enhance nighttime  $\text{O}_3$  depression at SSI. Figure 6c further presents corresponding variations of daytime (10:00–16:00 LST) and nighttime (23:00–04:00 LST) mean  $\text{O}_3$  concentrations at SSI. Both daytime and nighttime  $\text{O}_3$  concentrations exhibited downward changes, reflecting the  $\text{O}_3$  response to the



enhanced  $O_3$  diffusion and depression in September and October. Therefore, the enhanced diffusion and depression of  $O_3$  induced by the elevated wind speed and  $NO_x$  concentrations might be important causes of the observed  $O_3$  changes in September and October at SSI. It should be noted that the influence of radiation cannot be analyzed since observations of solar radiation were not available during the study period. Therefore, more measurements are still needed to further understand the  $O_3$  changes and corresponding drivers in the oceanic air.

### 3.4 Impacts of urban plumes on ozone in oceanic air at SSI

Due to the relatively long residence lifetime (about one month),  $O_3$  produced at urban regions could be transported several hundred kilometers away to downwind areas. Meanwhile, the urban plumes become more aged with continuous production/depletion of  $O_3$  and its precursors, resulting in non-linear changes in  $O_3$  in downwind areas (Geng et al., 2011; Tie et al., 2009, 2013). Several studies suggested that there tended to be considerable  $O_3$  formations in aged urban plumes in the downwind region of Shanghai (Geng et al., 2011; Tie et al., 2013). To investigate the impacts of urban plumes on the  $O_3$  levels in oceanic air at SSI, the relationships between observed  $O_3$  and  $NO_x$  under different wind conditions at SSI and DT are investigated in this section.

Figure 7 presents the daytime and nighttime  $O_3/NO_x$ -wind relationships in MAM (March–May), JJA (June–August), SON (September–November), and DJF (December–February), respectively during 2012–2017. The SW and W winds were associated with higher  $NO_x$  concentrations in both daytime and nighttime. The result was consistent with the observed CO changes in Sect. 3.1. Since there is no local anthropogenic emission at

SSI, the higher levels of  $\text{NO}_x$  and CO were mainly resulted from the transport of more polluted urban plumes by the SW and W winds. Generally, observed daytime  $\text{O}_3$  and  $\text{NO}_x$  concentrations presented opposite variations with the wind direction changes (Fig. 7a). In SON and DJF, the correlation coefficients ( $R_s$ ) between daytime  $\text{O}_3$  and  $\text{NO}_x$  were -0.72 and -0.75, respectively, indicating that the  $\text{O}_3$  formation was inhibited by increased  $\text{NO}_x$  concentrations. The results are in accordance with Tie et al. (2013) and Xu et al. (2019), who suggested that Shanghai and a broader regional area surrounding the city were all in the VOC-limited  $\text{O}_3$  formation regime during the study period. However, in MAM and JJA, the daytime  $\text{O}_3$ - $\text{NO}_x$  variations presented totally different patterns under SW and W wind conditions. As wind directions turned from E-SE to SW-W, observed mean  $\text{NO}_x$  concentrations increased from about 10 ppbv to 20 ppbv, while observed mean  $\text{O}_3$  concentrations increased from 50–60 ppbv to 70–80 ppbv. The enhancements in daytime  $\text{O}_3$  levels suggested that there should be persistent production of  $\text{O}_3$  in the polluted air masses carried by the SW and W winds in MAM and JJA.

Based on observations and WRF-Chem simulations, Tie et al. (2013) suggested considerable  $\text{O}_3$  production in aged city plumes in the downwind area of Shanghai. Since air masses affecting SSI site were directly originated from Shanghai under the SW and W wind conditions (Fig. 1), the observed  $\text{O}_3$  enhancements should be mainly attributed to the  $\text{O}_3$  production in the city plumes carried by SW and W winds. Studies during the MIRAGE-Shanghai campaign suggested several factors that contributed to the  $\text{O}_3$  enhancements in aged city plumes downwind Shanghai. First, as there is a large area of forest located in the south of Shanghai, Geng et al. (2011) suggested that continuous

oxidation of isoprene emitted by the biogenic sources could result in enhanced production of hydrogen radicals ( $\text{HO}_2$ ) especially in warm seasons. Once the air masses were transported north and mixed with high  $\text{NO}_x$  emissions,  $\text{O}_3$  would be quickly produced. However, the impacts of biogenic emissions on  $\text{O}_3$  production were mainly limited in the south part of Shanghai, which can hardly influence the atmosphere in the SSI region. Then, Tie et al. (2013) further illustrated that the OH reactivity of alkane, alkene, aromatics, and oxygenated VOCs (OVOCs) contributed to the  $\text{O}_3$  formation in city plumes. Among them, the influence of alkane, alkene and aromatics mostly occurred within or near the city, while the OVOCs could be produced or emitted during the transport of the city plumes, resulting in substantial  $\text{O}_3$  enhancements in aged city plumes at 100–200 km downwind Shanghai.

The SSI is located approximately 100 km northeast from the downtown area of Shanghai. In MAM and JJA, the SW and W winds carried air masses with enhanced OVOCs oxidation and  $\text{O}_3$  production, resulting in elevated daytime  $\text{O}_3$  levels on the island. While in SON and DJF, the observed  $\text{O}_3$  decreases at SSI during SW and W winds suggested lower efficiency of  $\text{O}_3$  productivity in the city plumes. That might be because that fewer OVOCs were released or produced downwind the city due to the lower temperature and weaker solar radiation (Cai et al., 2009). In addition, in SON and DJF, the SW and W winds were usually related to low pressure system with large cloud cover and rich water vapor in Shanghai, which could also lead to depressed photochemical reactions and decreased  $\text{O}_3$  levels. At night, observed  $\text{O}_3$  and  $\text{NO}_x$  displayed totally opposite changes with wind directions (Fig. 7b), indicating  $\text{O}_3$  depression by nighttime  $\text{NO}_x$  titration

in all the seasons. High  $O_3$  levels were observed under northeasterly, easterly and southeasterly oceanic wind conditions, ranging from 50–60, 30–55, 55–60, and 40–50 ppbv respectively at night in MAM, JJA, SON, and DJF.

### 3.5 Impacts of offshore ozone on urban ozone air quality in Shanghai

As is presented in Sect. 3.2 and 3.3, observed  $O_3$  concentrations at SSI were much higher than those at urban site (XJH), suggesting higher levels of  $O_3$  in oceanic air than those on the continent. Therefore, sea breezes tend to bring more  $O_3$  to the continent, aggravating  $O_3$  pollution in coastal cities. Shanghai is one of the largest cities located on the east coast of China, experiencing severe  $O_3$  pollution in recent years (Xu et al., 2019; Gu et al., 2020). According to the cluster analysis results (Fig. S2), easterly winds from the ocean greatly affected the Shanghai region, accounting for 64–78% of the total flows in non-winter months during the period 2012–2017. To understand the impacts of higher  $O_3$  in oceanic air on the urban air quality, numerical experiments are conducted using the WRF-Chem model to examine the response of  $O_3$  levels in Shanghai to various oceanic air inflow conditions in this section.

Simulations are performed during September 1–30 2014 when the prevailing winds were mostly northeasterly and easterly in the Shanghai region. The occurrence frequencies of the northeasterly and easterly winds were 23% and 27% respectively, during the simulation period, suggesting dominant influence of the oceanic air inflows on the city of Shanghai. Consistent with above analysis, observed air  $O_3$  concentrations were much higher in oceanic regions than those in city areas, with monthly mean values of 30.9 and 57.7 ppbv, respectively at XJH and SSI in September 2014. The chemical boundary

conditions (BCs) of the regional model can represent the inflows conditions to explore their impacts on surface concentrations of air pollutants over a certain continent region. Using this method, Pfister et al. (2011) proposed that chemical inflows taken from different observational and model datasets could result in differences of  $\pm 15$  ppbv in  $O_3$  levels in the US west coast region. Therefore, three sets of numerical experiments are conducted as follows to assess the impacts of oceanic  $O_3$  air inflows on the urban  $O_3$  air quality in Shanghai. All the simulations are driven by the same emissions, initial conditions, physical and chemical schemes.

(1) BC\_40:  $O_3$  concentrations at the eastern lateral boundary of the domain on the ocean are assigned to 40 ppbv, which is provided by the MOZART-4 model, closed to the observed urban  $O_3$  levels (29.0–38.4 ppbv) in Shanghai in September. The chemical BCs are updated every 6 hours.

(2) BC\_50: Same as BC\_40, but with  $O_3$  concentrations setting to 50 ppbv at the eastern lateral boundary of the domain.

(3) BC\_60: Same as BC\_40, but with  $O_3$  concentrations at the eastern lateral boundary of the domain setting to 60 ppbv according to the observed  $O_3$  levels at SSI (50.9–71.0 ppbv) in September.

Figure 8 displays the simulated and observed monthly mean distributions of surface  $O_3$  concentrations in BC\_40, BC\_50 and BC\_60 scenarios, respectively. In addition to the observations at XJH and SSI,  $O_3$  measurements obtained from other three sites, Pudong (PD, suburban), Sheshan (SS, rural), and Dongtan (DT, rural), during the same period were introduced to evaluate the model's performance in simulating  $O_3$  in Shanghai. The

O<sub>3</sub> concentrations at all the sites were measured using the same method as described in Sect. 2.1. The calculated distributions of O<sub>3</sub> agree with observations, which exhibit lower values in urban regions compared to those in rural and ocean areas, indicating strong O<sub>3</sub> depressions in the city of Shanghai due to the VOC-limited O<sub>3</sub> formation regime. The R values between the simulated and observed O<sub>3</sub> concentrations are all larger than 0.50 at continental sites (XJH, PD, SS, and DT), suggesting good prediction of O<sub>3</sub> variations by the model.

Table 4 displays the statistical results of the comparisons between the simulated and observed surface O<sub>3</sub> concentrations at different sites in Shanghai. Generally, the WRF-Chem model underestimates O<sub>3</sub> concentrations at all the sites in most cases. Taken the BC\_40 scenario for example, the O<sub>3</sub> concentrations are underestimated by 9.4–27.6% at continental sites and 36.1% at SSI, suggesting larger underestimation of O<sub>3</sub> concentrations in oceanic regions. Model results further suggest that elevated O<sub>3</sub> levels in the eastern chemical BCs would lead to increases in O<sub>3</sub> concentrations at both urban and remote sites when the prevailing winds are mostly easterly in Shanghai. With O<sub>3</sub> concentrations increasing from 40 to 60 ppbv in the easterly oceanic air inflows, the simulated monthly mean O<sub>3</sub> concentrations increase by 7.0–9.7 ppbv at continental sites and 10.4 ppbv at SSI. The underestimation of O<sub>3</sub> levels by the model is also greatly improved in the BC\_60 scenario, when the chemical BCs of O<sub>3</sub> are more close to the observations. Compared to those in the BC\_40 scenario, the normalized mean bias (NMBs) of the predicted O<sub>3</sub> concentrations reduced at most sites in the BC\_60 scenario, for example from -36.1 % to -18.1 % at SSI and -27.6% to -4.6% at XJH, suggesting a

crucial role of the eastern oceanic air inflows in influencing O<sub>3</sub> air quality in Shanghai.

The calculated monthly mean differences in surface O<sub>3</sub> concentrations between simulations in different scenarios are further presented in Fig. 9. Since the dominant winds are easterly during the simulation period, distinct changes in surface O<sub>3</sub> concentrations throughout Shanghai are generated, exhibiting generally gradient increases from the ocean to the continent as O<sub>3</sub> increases in the oceanic air inflows. With every 10 ppbv increases in O<sub>3</sub> levels in oceanic air, the simulated surface mean O<sub>3</sub> concentrations increase by 3–6 ppbv in the land area and 4–7 ppbv in the offshore region. Due to the strong O<sub>3</sub> depressions associated with high anthropogenic emissions, the simulated O<sub>3</sub> enhancements are relatively lower in the central urban region compared to those in surrounding areas. Even so, simulated mean O<sub>3</sub> concentrations still exhibit 6–8 ppbv increases in downtown Shanghai in the BC<sub>60</sub> scenario, accounting for approximately 30% of the simulated O<sub>3</sub> concentrations in the BC<sub>40</sub> case. During the period 2012–2017, most of the measured O<sub>3</sub> concentrations ranged between 50–60 ppbv at SSI in non-winter seasons. Carried by the easterly inflows, these oceanic air masses with higher O<sub>3</sub> levels (50–60 ppbv) could be transported to the coastal regions, resulting in approximately 20–30% increases in urban O<sub>3</sub> concentrations in Shanghai according to the sensitivity results.

#### 4 Conclusions

In this paper, we present the first relatively long and continuous measurements of oceanic air O<sub>3</sub> conducted at an offshore monitoring station on the Sheshan Island during January 1 2012 to September 15 2017. The southwesterly and westerly winds are proved to carry more pollutants to the SSI site, exerting greater influence of human activities on the

oceanic atmosphere over the offshore region of the East China Sea. Since the two kinds of winds exhibited minimum occurrence frequencies and wind speeds in September and October, atmosphere at SSI during the two months are considered to be less affected by the transport of regional pollution.

Compared to those in urban (XJH) and rural (DT) sites, the observed  $O_3$  levels were higher at SSI, with a mean value of 50.1 ppbv during the observation period. Similar seasonal and diurnal patterns of  $O_3$  were observed at SSI and XJH; however, the amplitudes of  $O_3$  variations were much smaller at the offshore site (SSI). Since  $O_3$  formation in Shanghai and its surrounding regions were VOC-limited, the observational results suggested that the production and depression of  $O_3$  could be weaker in the ocean regions due to weak influence of the anthropogenic emissions. Observed mean  $O_{3-max}/O_{3-min}$  ratios also exhibited lower values at SSI (3.03) than those at XJH (5.20), with minimum values ranging from 1.61–2.35 in September and October. The result further illustrated that SSI was seldom affected by the anthropogenic emissions, especially in September and October.

The multi-year changes of the oceanic  $O_3$  at SSI are investigated using the Mann-Kendall trend test and the Theil-Sen trend estimate method during 2012–2017. Different from the significant  $O_3$  increases detected at XJH and other rural sites reported in previous studies, the observed mean  $O_3$  concentrations at SSI exhibited statistically insignificant increasing changes ( $1.12 \text{ ppbv yr}^{-1}$ ,  $\alpha > 0.10$ ) during the observation period and insignificant decreasing changes ( $-0.72 \text{ ppbv yr}^{-1}$ ,  $\alpha > 0.10$ ) in September and October when the transport of city pollutants had minimum impacts on the island. Due to fewer



impacts of anthropogenic emissions, most of the observed changes in  $O_3$  at SSI could be attributed to the changes of meteorological conditions. Observed wind speed exhibited significant increases ( $0.21 \text{ m s}^{-1} \text{ yr}^{-1}$ ,  $\alpha < 0.05$ ) in September and October during the observation period, suggesting that enhanced diffusion conditions could be an important meteorological factor in determining the decreases in  $O_3$  concentrations during the observation period.

The impacts of urban plumes on  $O_3$  levels in oceanic air at SSI are evaluated by studying the relationships between observed  $O_3$  and  $NO_x$  under different wind conditions. The SW and W winds usually carried air masses with higher  $NO_x$  concentrations in both daytime and nighttime to the island. Generally, observed daytime and nighttime  $O_3$  concentration decreased as  $NO_x$  concentration increases in SW and W winds, exhibiting typical VOC-limited characteristics of  $O_3$  formation. The pattern was more typical in SON and DJF, with R values of -0.72 and -0.75, respectively between  $O_3$  and  $NO_x$  concentrations. In MAM and JJA, the daytime  $O_3$ - $NO_x$  variations presented kind of positive relationships under SW and W wind conditions, suggesting continuous  $O_3$  production in aged city plumes from Shanghai. As reported in previous studies during the MIRAGE-Shanghai campaign, enhanced OVOCs oxidation should be the most important driver of the observed  $O_3$  enhancements in the city plumes transported by the SW and W winds.

The influence of the oceanic  $O_3$  air inflows on urban  $O_3$  air quality in Shanghai are quantified during an easterly wind dominant episode (September 1–30, 2014). Numerical experiments are conducted with chemical BCs of  $O_3$  assigned according to different inflow

conditions using the WRF-Chem model. Model results suggest that increases of  $O_3$  in the easterly oceanic air inflows will lead to gradient increases from the ocean to the continent. With every 10 ppbv  $O_3$  increases, the calculated surface mean  $O_3$  concentrations can increase by 3–6 ppbv in the land and 4–7 ppbv in the offshore region. Compared to those in surrounding regions,  $O_3$  in central city of Shanghai exhibited lower enhancements in response to the  $O_3$  increases in oceanic air inflows due to strong  $O_3$  depression processes. Even so, the impacts of the oceanic air inflows can still lead to 20–30% increases in urban  $O_3$  concentrations which should be crucially considered in dealing with  $O_3$  pollution in large coastal cities like Shanghai.

*Data availability.* The data used in this paper can be provided upon request from Dr. Jianming Xu (metxujm@163.com).

*Author contribution.* YG and JX came up with the original idea, designed the analysis methods, developed the model code, and performed the simulations. WG provided the observational data. YG and YQ conducted the analysis of the observations and model results. YG prepared the manuscript with contributions from all co-authors.

*Competing interest.* The authors declare that they have no conflict of interest.

*Acknowledgements.* This work was supported by Shanghai Sailing program (18YF1421200) and Science and Technology Commission of Shanghai Municipality

563 (Grand No. 19DZ1205003).

## Reference

- Cai, C., Geng, F., Tie, X. X., Yu, Q., and An, J.: Characteristics and source apportionment of VOCs measured in Shanghai, China, *Atmos. Environ.*, 44, 5005–5014, 2010.
- Chen, F. and Dudhia, J.: Coupling an advanced land surface hydrology model with the Penn State-NCAR MM5 modeling system, Part I: Model implementation and sensitivity, *Mon. Weather Rev.*, 129, 569–585, 2001.
- Cvitas, T., and Klasinc, L.: Measurement of tropospheric ozone in the Eastern Mediterranean, *Boll. Geofisico*, 16, 521–527, 1993.
- Cvitas, T., Kezele, N., Klasinc, L., and Lisac, J.: Tropospheric ozone measurements in Croatia, *Pure Appl. Chem.*, 67, 1450–1453, 1995.
- Draxler, R. R. and Hess, G. D.: An overview of the HYSPLIT 4 modelling system for trajectories, dispersion, and deposition, *Austral. Meteorol. Mag.*, 47, 295–308, 1998.
- Dudhia, J.: Numerical study of convection observed during the winter monsoon experiment using a mesoscale two-dimensional model, *J. Atmos. Sci.*, 46, 3077–3107, 1989.
- Emmons, L. K., Walters, S., Hess, P. G., Lamarque, J.-F., Pfister, G. G., Fillmore, D., Granier, C., Guenther, A., Kinnison, D., Laepple, T., Orlando, J., Tie, X., Tyndall, G., Wiedinmyer, C., Baughcum, S. L., and Kloster, S.: Description and evaluation of the Model for Ozone and Related chemical Tracers, version 4 (MOZART-4), *Geosci. Model Dev.*, 3, 43–67, <https://doi.org/10.5194/gmd-3-43-2010>, 2010.
- Fountoukis, C., and Nenes, A.: ISORROPIA II: a computationally efficient aerosol thermodynamic equilibrium model for  $K^+$ ,  $Ca^{2+}$ ,  $Mg^{2+}$ ,  $NH_4^+$ ,  $Na^+$ ,  $SO_4^{2-}$ ,  $NO_3^-$ ,  $Cl^-$ ,  $H_2O$  aerosols. *Atmos. Chem. Phys.* 7, 4639–4659, 2007.
- Fu, Y., Liao, H., and Yang Y.: Interannual and Decadal Changes in Tropospheric Ozone in China and the Associated Chemistry-Climate Interactions: A Review, *Adv. Atmos. Sci.*, 46, 452–460, 2019.
- Gao, W., Tie, X., Xu, J., Huang, R., Mao, X., Zhou, G., and Chang, L.: Long-term trend of  $O_3$  in a mega city (Shanghai), China: characteristics, causes, and interactions with precursors, *Sci. Total Environ.*, 603–604, 425–433, 2017.
- Geng, F., Mao, X., Zhou, M., Zhong, S., and Lenschow, D.: Multi-year ozone concentration and its spectra in Shanghai, China, *Sci. Total Environ.*, 521–522, 135–143, 2015.
- Geng, F., Tie, X., Guenther, A., Li, G., Cao, J., and Harley, P.: Effect of isoprene emissions from major forests on ozone formation in the city of Shanghai, China, *Atmos. Chem. Phys.*, 11, 10449–10459, 2011.
- Gilbert, R.O.: *Statistical Methods for Environmental Pollution Monitoring*. John Wiley & Sons, New York, USA, 1987.
- Goodman, J. E., Prueitt, R. L., Sax, S. N., Pizzurro, D. M., Lynch, H. N., Zu, K., and Venditti, F. J.: Ozone exposure and systemic biomarkers: evaluation of evidence for adverse cardiovascular health impacts, *Crit. Rev. Toxicol.*, 45, 412–452, 2015.
- Grell, G. A., Peckham, S. E., Schmitz, R., McKeen, S. A., Frost, G., Skamarock, W. C., and Eder, B.: Fully coupled “online” chemistry within the WRF model, *Atmos. Environ.*, 39, 6957–6975, 2005.

- Gocic, M., Trajkovic, S.: Analysis of changes in meteorological variables using Mann-Kendall and Sen's slope estimator statistical tests in Serbia, *Global Planet. Change*, 100, 172–182, 2013.
- Gu, Y., Li, K., Xu, J., Liao, H., Zhou, G.: Observed dependence of surface ozone on increasing temperature in Shanghai, China. *Atmos. Environ.*, 221, 117108, 2020.
- Guenther, A., Karl, T., Harley, P., Wiedinmyer, C., Palmer, P. I., and Geron, C.: Estimates of global terrestrial isoprene emissions using MEGAN (model of emissions of gases and aerosols from nature), *Atmos. Chem. Phys.*, 6, 3181–3210, 2006.
- Hong, S. Y. and Lim, J. O. J.: The WRF Single-Moment 6-Class Microphysics Scheme (WSM6), *J. Korean Meteor. Soc.*, 42, 129–151, 2006.
- IPCC: Climate Change 2013: The Physical Science Basis. Contribution of Working Group I to the Fifth Assessment Report of the Intergovernmental Panel on Climate Change, edited by Stocker, T. F., Qin, D., Plattner, G. K., Tignor, M., Allen, S. K., Boschung, J., Nauels, A., Xia, Y., Bex, V. and Midgley, P. M., Cambridge University Press, United Kingdom and New York, USA, 2013.
- Kendall, M.G.: Rank Correlation Methods, fourth ed., Charles Griffin, London, 1975.
- Li, K., Jacob, D.J., Liao, H., Zhu, J., Shah, V., Shen, L., Bates, K.H., Zhang, Q., and Zhai, S.: A two-pollutant strategy for improving ozone and particulate air quality in China. *Nat. Geosci.* <https://doi.org/10.1038/s41561-019-0464-x>, 2019a.
- Li, K., Jacob, D. J., Liao, H., Shen, L., Zhang, Q., and Bates, K.H.: Anthropogenic drivers of 2013–2017 trends in summer surface ozone in China, *P. Natl. A. Sci. USA* 116 (2), 422–427, 2019b.
- Li, M., Zhang, Q., Streets, D., He, K. B., Cheng, Y. F., Emmons, L. K., Huo, H., Kang, S. C., Lu, Z., Shao, M., Su, H., Yu, X., and Zhang, Y.: Mapping Asian anthropogenic emissions of non-methane volatile organic compounds to multiple chemical mechanisms. *Atmos. Chem. Phys.* 14, 5617–5638, 2014.
- Lin, M., Horowitz, L. W., Cooper, O. R., Tarasick, D., Conley, S., Iraci, L. T., Johnson, B., Leblanc, T., Petropavlovskikh, I., and Yates, E. L.: Revisiting the evidence of increasing springtime ozone mixing ratios in the free troposphere over western North America, *Geophys. Res. Lett.*, 42, 8719–8728, <https://doi.org/10.1002/2015GL065311>, 2015.
- Lin, Y. L., Farley, R. D., and Orville, H. D.: Bulk parameterization of the snowfield in a cloud model, *J. Clim. Appl. Meteorol.*, 22, 1065–1092, 1983.
- Lin, W., Xu, X., Zhang, X., Tang, J.: Contributions of pollutants from North China Plain to surface ozone at the Shangdianzi GAW Station, *Atmos. Chem. Phys.*, 8, 5889–5898, 2008.
- Lou, S., Liao, H., Yang, Y., and Mu, Q., Simulation of the interannual variations of tropospheric ozone over China: Roles of variations in meteorological parameters and anthropogenic emissions, *Atmos. Environ.*, 122, 839–851, 2015.
- Lu, X., Hong, J., Zhang, L., Cooper, O.R., Schults, M. G., Xu, X., Wang, T., Gao, M., Zhao, Y., and Zhang, Y.: Severe surface ozone pollution in China: a global perspective, *Environ. Sci. Technol. Lett.*, 5(8), 487, 194, 2018.
- Ma, Z., Xu, J., Quan, W., Zhang, Z., Lin, W., and Xu, X.: Significant increase of surface ozone at a rural site, north of eastern China, *Atmos. Chem. Phys.*, 16, 3969–3977,

2016.

Madronich, S., and Flocke, S.: The role of solar radiation in atmospheric chemistry, in: Handbook of Environmental Chemistry, edited by Boule, P., Springer, Heidelberg, 1–26, [https://doi.org/10.1007/978-3-540-69044-3\\_1](https://doi.org/10.1007/978-3-540-69044-3_1), 1999.

Mann, H.B.: Non-parametric tests against trend, *Econometrica* 13, 163–171, 1945.

Meng, Z. Y., Xu, X. B., Yan, P., Ding, G. A., Tang, J., Lin, W. L., Xu, X. D., and Wang, S. F.: Characteristics of trace gaseous pollutants at a regional background station in Northern China, *Atmos. Chem. Phys.*, 9, 927–936, <https://doi.org/10.5194/acp-9-927-2009>, 2009.

Monks, P. S., Archibald, A. T., Colette, A., Cooper, O., Coyle, M., Derwent, R., Fowler, D., Granier, C., Law, K.S., Mills, G.E., Stevenson, D.S., Tarasova, O., Thouret, V., von Schneidmesser, E., Sommariva, R., Wild, O., and Williams, M.L.: Tropospheric ozone and its precursors from the urban to the global scale from air quality to short-lived climate forcer, *Atmos. Chem. Phys.*, 15, 8889–8973, 2015.

Pfister, G. G., Parrish, D. D., Worden, H., Emmons, L. K., Edwards, D. P., Wiedinmyer, C., Diskin, G. S., Huey, G., Oltmans, S. J., Thouret, V., Weinheimer, A., and Wisthaler, A.: Characterizing summertime chemical boundary conditions for airmasses entering the US West Coast, *Atmos. Chem. Phys.*, 11, 1769–1790, 2011.

Scheel, H. E., Aresbough, H., Geiss, H., Gormiscek, B., Granby, K., Haszpra, L., Klasinc, L., Kley, D., Laurila, T., Lindskog, A., Roemer, M., Schmitt, R., Simmond, P., Solberg, S., and Toupande, G.: On the spatial distribution and seasonal variation of lower tropospheric ozone over Europe, *J. Atmos. Chem.*, 28, 11–28, 1997.

Schell, B., Ackermann, I., Hass, H., Binkowski, F. S., and Ebel, A.: Modeling the formation of secondary organic aerosol within a comprehensive air quality model system, *J. Geophys. Res.*, 106, 28275–28293, <https://doi.org/10.1029/2001JD000384>, 2001.

Sen, P. K.: Estimates of the regression coefficient based on Kendall's tau, *J. Am. Stat. Assoc.*, 63, 1379–1389, 1968.

Shan, W., Yang, P., Lu, H., Ma, K., and Huang, Z.: Influence of Coastal Wind on Surface Ozone and Nitrogen Oxides in Suburban Shanghai, *Asia-Pac. J. Atmos. Sci.*, 52(5), 451–458, 2016.

Sillman, S.: Photochemical Smog: Ozone and its Precursors, in: Handbook of Weather, Climate, and Water, edited by Potter, T. and Bradley, R. R., John Wiley & Sons, New York, USA, 227–242, 2003.

Stockwell, W. R., Middleton, P., Chang, J. S., and Tang, X.: The second generation regional acid deposition model chemical mechanism for regional air quality modeling, *J. Geophys. Res.-Atmos.*, 95, 16343–16367, 1990.

Tie, X., Brasseur, G., Emmons, L., Horowitz, I., and Kinnison, D.: Effects of aerosols on tropospheric oxidants: a global model study, *J. Geophys. Res.-Atmos.*, 106, 22931–22964, 2001.

Tie, X., Geng, F., Guenther, A., Cao, J., Greenberg, J., Zhang, R., Apel, E., Li, G., Weinheimer, A., Chen, J., and Cai, C.: Megacity impacts on regional ozone formation: observations and WRF-Chem modeling for the MIRAGE-Shanghai field campaign, *Atmos. Chem. Phys.*, 13, 5655–5669, 2013.

Tie, X., Geng, F., Peng, L., Gao, W., and Zhao, C.: Measurement and modeling of O<sub>3</sub>

- variability in Shanghai, China: Application of the WRF-Chem model, *Atmos. Environ.*, 43, 4289–4302, 2009.
- Tie, X., Madronich, S., Li, G. H., Ying, Z.M., Weinheimer, A., Apel, E., and Campos, T.: Simulation of Mexico City plumes during the MIRAGE-Mex field campaign using the WRF-Chem model, *Atmos. Chem. Phys.* 9, 4621–4638, 2009.
- Tie, X., Madronich, S., Walters, S., Rasch, P., and Collins, W.: Effect of clouds on photolysis and oxidants in the troposphere, *J. Geophys. Res.*, 108, 4642, 2003.
- Vingarzan, R.: A review of surface ozone background levels and trends, *Atmos. Environ.*, 38, 3431–3442, 2004.
- Wang, T., Wei, X. L., Ding, A. J., Poon, C. N., Lam, Y. S., Li, Y. S., Chan, L. Y., and Anson, M.: Increasing surface ozone concentrations in the background atmosphere of Southern China, 1994–2007, *Atmos. Chem. Phys.*, 9, 6217–6227, 2009.
- Wang, T., Xue, L., Brimblecombe, P., Lam, Y.-F., Li, L., and Zhang, L.: Ozone pollution in China: A review of concentrations, meteorological influences, chemical precursors, and effects, *Sci. Total Environ.*, 575, 1582–1596, 2017.
- Wesely, M. L.: Parameterization of surface resistances to gaseous dry deposition in regional-scale numerical models, *Atmos. Environ.*, 23, 1293–1304, 1989.
- Xu, J., Tie, X., Gao, W., Lin, Y., and Fu, Q.: Measurement and model analyses of the ozone variation during 2006 to 2015 and its response to emission change in megacity Shanghai, China, *Atmos. Chem. Phys.*, 19, 9017–9035, 2019.
- Xu, X., Lin, W., Wang, T., Yan, P., Tang, J., Meng, Z., and Wang, Y.: Long-term trend of surface ozone at a regional background station in eastern China 1991–2006: enhanced variability, *Atmos. Chem. Phys.*, 8, 2595–2607, 2008.
- Xu, W., Lin, W., Xu, X., Tang, J., Huang, J., Wu, H., and Zhang, X.: Long-term trends of surface ozone and its influencing factors at the Mt Waliguan GAW station, China – part 1: overall trends and characteristics, *Atmos. Chem. Phys.*, 16, 6191–6205, <https://doi.org/10.5194/acp-16-6191-2016>, 2016.
- Yang, Y., Liao, H., and Li, J., Impacts of the East Asian summer monsoon on interannual variations of summertime surface-layer ozone concentrations over China, *Atmos. Chem. Phys.*, 14, 6867–6880, 2014.
- Yue, X. and Unger, N.: Ozone vegetation damage effects on gross primary productivity in the United States, *Atmos. Chem. Phys.*, 14, 9137–9153, 2014.

727 Table 1 Mean CO mixing ratios (ppmv) under north (N), northeast (NE), east (E),  
 728 southeast (SE), south (S), southwest (SW), west (W), northwest (NW) and calm (C) wind  
 729 conditions at Dongtan (DT) site, a remote rural site near the Sheshan Island (SSI) during  
 730 2012 to 2017.

	N	NE	E	SE	S	SW	W	NW	C
CO	0.31	0.27	0.25	0.23	0.27	<b>0.44</b>	<b>0.56</b>	0.38	0.34



731 Table 2 Monthly mean wind speeds ( $\text{m s}^{-1}$ ) and occurrence frequencies (%) of the  
 732 southwest (SW) and west (W) winds at Dongtan (DT) site, a remote rural site near the  
 733 Sheshan Island (SSI) during 2012 to 2017.

	Jan.	Feb.	Mar.	Apr.	May	Jun.	Jul.	Aug.	Sep.	Oct.	Nov.	Dec.
SW+W	11.5	9.2	11.9	13.2	12.7	9.8	17.7	10.8	<b>6.1</b>	<b>5.2</b>	11.9	15.1
Wind speed	2.70	2.93	2.98	3.04	2.86	2.51	2.65	2.77	<b>2.49</b>	<b>2.50</b>	2.55	2.54

Table 3 Statistical results of the Mann-Kendall test and Theil-Sen trend estimate for daily mean values of NO<sub>x</sub>, CO mixing ratios, temperature (T), and wind speed (WS) in September and October at Dongtan (DT) site, a remote rural site near Sheshan Island (SSI) site during the 2012–2017 period. The units of the calculated slopes are ppbv yr<sup>-1</sup> for NO<sub>x</sub> and CO, °C yr<sup>-1</sup> for T, and m s<sup>-1</sup> yr<sup>-1</sup> for WS.

	NO <sub>x</sub>	CO	T	WS
Slope Estimate	0.48*	2.67 <sup>Δ</sup>	0.15 <sup>Δ</sup>	0.21*

\*The result is significant at the 95% confidence level.

<sup>Δ</sup>The result cannot pass the Mann-Kendall trend test at the 90% confidence level.

Table 4 Statistical results of the comparisons between the simulated and observed surface O<sub>3</sub> concentrations at Sheshan (SS), Xujiahua (XJH), Pudong (PD), DT (Dongtan) and Sheshan Island (SSI) sites during September 2014. The calculated O<sub>3</sub> levels are obtained from BC\_40, BC\_50 and BC\_60 simulations, respectively. Values of the average surface O<sub>3</sub> concentrations (Mean) and normalized mean bias (NMB) are displayed. The NMB is defined as  $NMB = \frac{\sum_{i=1}^n (P_i - O_i)}{\sum_{i=1}^n O_i}$ , where  $P_i$  and  $O_i$  are predicted and observed ozone mixing ratios for sample  $i$ ,  $n$  is the number of total samples (numbers in parentheses).

	Cases	SS (681)	XJH (641)	PD (690)	DT (690)	SSI (720)
	Observation	39.7	30.4	40.3	46.4	57.7
Mean	BC_40	36.0	22.0	29.5	35.3	36.9
(ppbv)	BC_50	39.1	25.1	33.3	39.6	41.8
	BC_60	43.1	29.0	37.9	45.0	47.3
	BC_40	-9.4	-27.6	-26.7	-23.9	-36.1
NMB(%)	BC_50	-1.5	-17.5	-17.2	-14.5	-27.5
	BC_60	8.6	-4.6	-5.9	-3.0	-18.1

## Figure Captions

**Figure 1** Land cover of Shanghai and corresponding locations and landscapes of Xujiahui (XJH, urban), Dongtan (DT, rural) and Sheshan Island (SSI, remote and oceanic) stations.

**Figure 2** Monthly wind rose diagrams averaged over the period of 2012 to 2017 at Dongtan (DT) site, a remote rural site near the Sheshan Island (SSI).

**Figure 3** Monthly mean CO mixing ratios under north (N), northeast (NE), east (E), southeast (SE), south (S), southwest (SW), west (W), northwest (NW) and calm (C) wind conditions at Dongtan (DT) site, a remote rural site near the Sheshan Island (SSI) during 2012 to 2017.

**Figure 4** Monthly and year-round mean diurnal variations of O<sub>3</sub> (ppbv) at Sheshan Island (SSI, remote and oceanic) and Xujiahui (XJH, urban) sites during 2012 to 2017.

**Figure 5** Calculated monthly mean ratios of daily maximum O<sub>3</sub> concentrations (O<sub>3-max</sub>) to minimum O<sub>3</sub> concentrations (O<sub>3-min</sub>) at Sheshan Island (SSI, remote and oceanic) and Xujiahui (XJH, urban) sites, respectively during 2012 to 2017.

**Figure 6** Variations of (a) monthly mean O<sub>3</sub> concentrations at Sheshan Island (SSI, remote and oceanic) and Xujiahui (XJH, urban) sites during the period 2012–2017, (c) corresponding variations of daily mean O<sub>3</sub> concentrations at SSI and XJH in September and October, and (c) variations of mean O<sub>3</sub> concentrations during daytime (10:00-16:00 LST) and nighttime (23:00-04:00 LST) at SSI.

**Figure 7** Daytime and nighttime mean O<sub>3</sub> mixing ratios (ppbv) at Sheshan Island (SSI) and NO<sub>x</sub> mixing ratios (ppbv) at Dongtan (DT) site, a remote rural site near SSI under north (N), northeast (NE), east (E), southeast (SE), south (S), southwest (SW), west (W),

and northwest (NW) wind conditions in MAM (March–May), JJA (June–August), SON (September–November), and DJF (December–February), respectively during 2012 to 2017.

**Figure 8** Calculated distributions of monthly mean O<sub>3</sub> concentrations (shades, ppbv) from BC\_40, BC\_50 and BC\_60 simulations, respectively in September 2014. Model results are compared with observed mean O<sub>3</sub> concentrations (circles, ppbv) obtained from Sheshan (SS), Xujiahua (XJH), Pudong (PD), DT (Dongtan) and Sheshan Island (SSI) sites. Also shown is the calculated wind field (m s<sup>-1</sup>) averaged over the same period.

**Figure 9** Mean differences in surface O<sub>3</sub> concentrations (ppbv) simulated with different chemical boundaries: (a) BC\_50 minus BC\_40, (b) BC\_60 minus BC\_40, and (c) BC\_60 minus BC\_50 in September 2014. Also shown is the calculated wind field (m s<sup>-1</sup>) averaged over the simulation period.

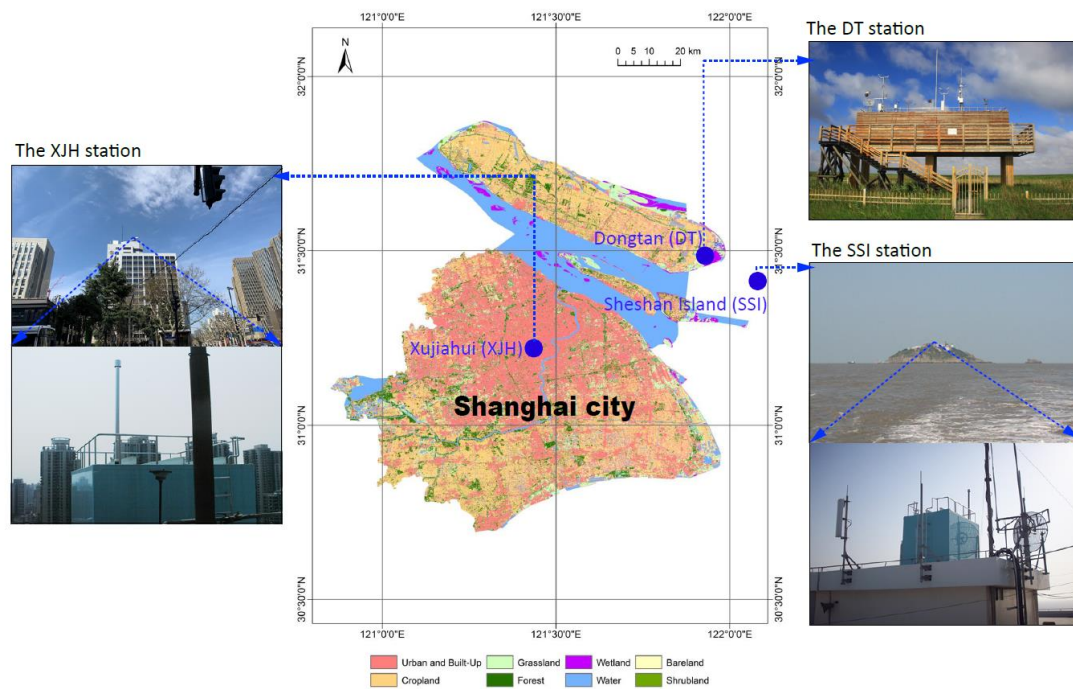


Figure 1 Land cover of Shanghai and corresponding locations and landscapes of Xujiahui (XJH, urban), Dongtan (DT, rural) and Sheshan Island (SSI, remote and oceanic) stations.

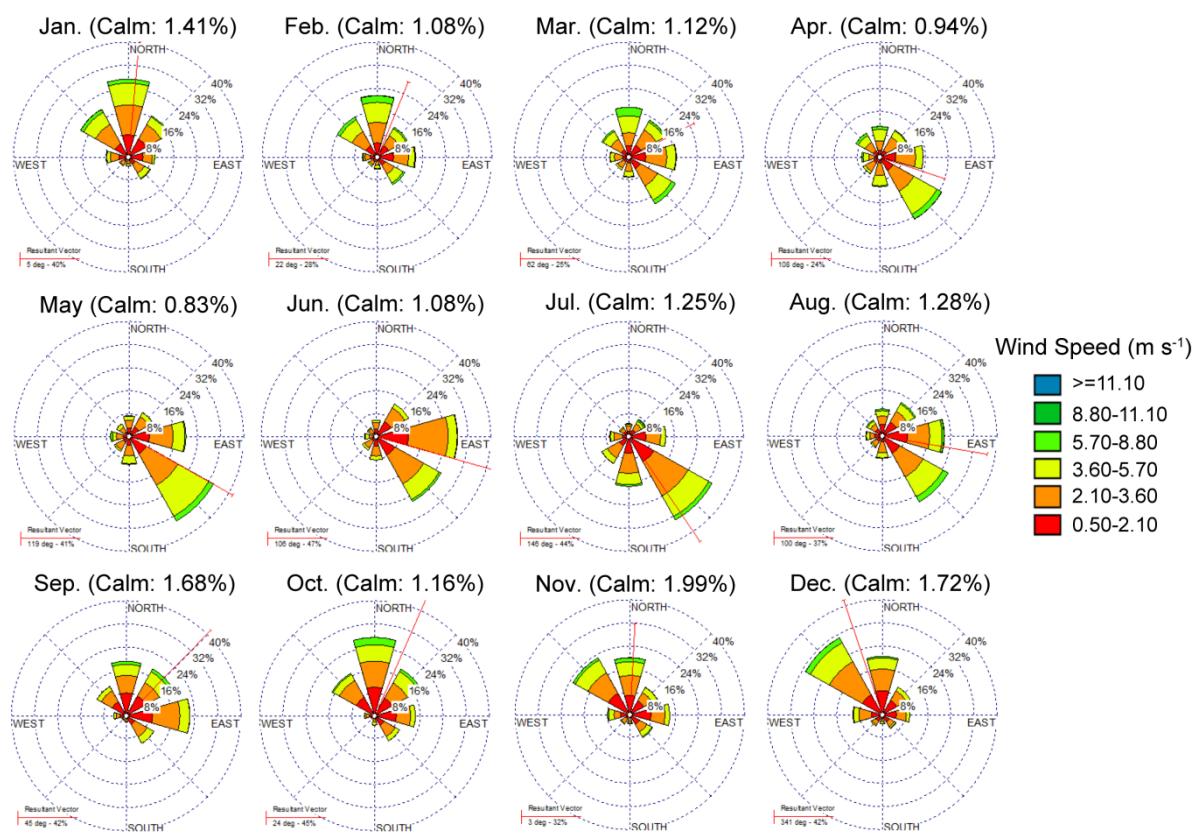


Figure 2 Monthly wind rose diagrams averaged over the period of 2012 to 2017 at Dongtan (DT) site, a remote rural site near the Sheshan Island (SSI).

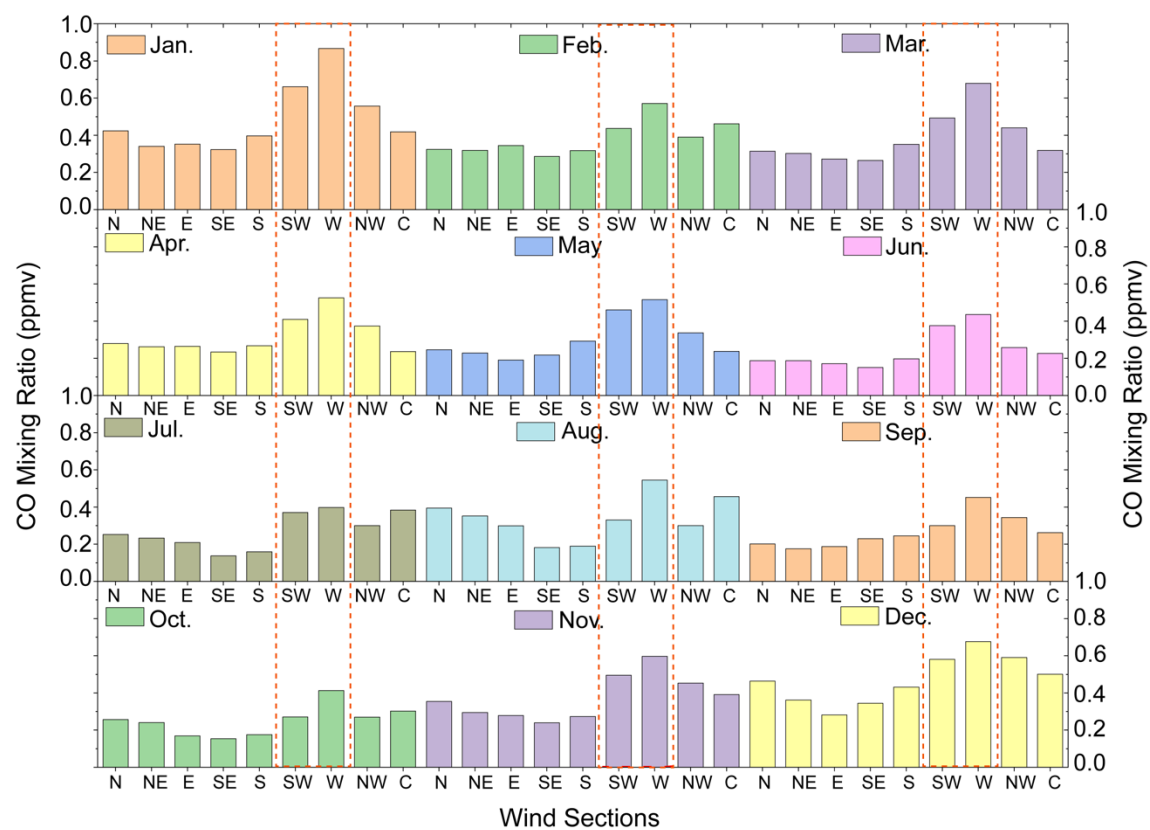


Figure 3 Monthly mean CO mixing ratios under north (N), northeast (NE), east (E), southeast (SE), south (S), southwest (SW), west (W), northwest (NW) and calm (C) wind conditions at Dongtan (DT) site, a remote rural site near the Sheshan Island (SSI) during 2012 to 2017.



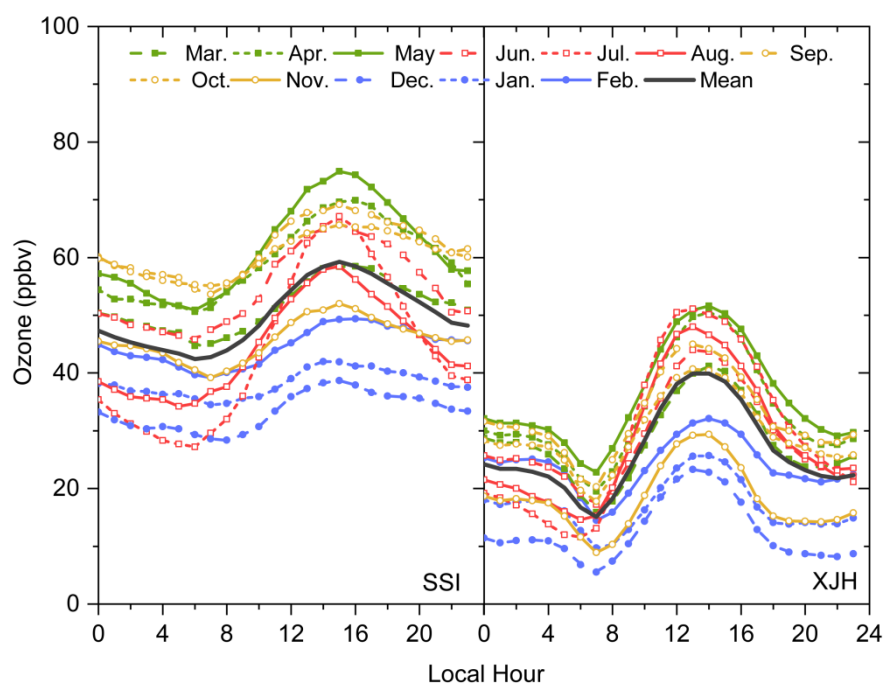


Figure 4 Monthly and year-round mean diurnal variations of  $O_3$  (ppbv) at Sheshan Island (SSI, remote and oceanic) and Xujianghai (XJH, urban) sites during 2012 to 2017.

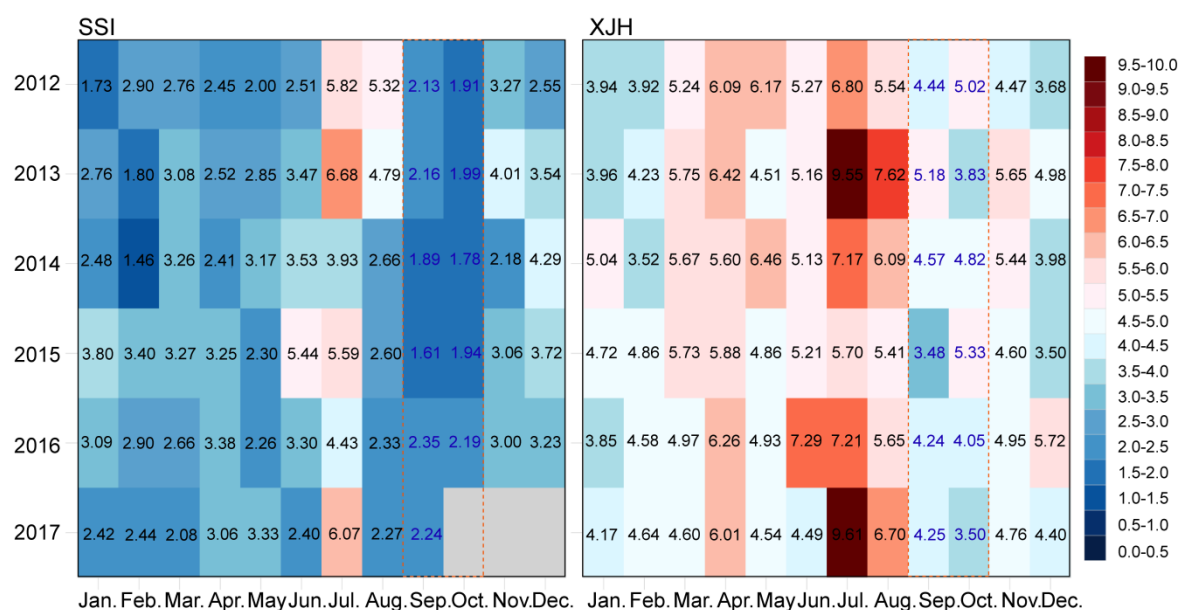


Figure 5 Calculated monthly mean ratios of daily maximum O<sub>3</sub> concentrations (O<sub>3-max</sub>) to minimum O<sub>3</sub> concentrations (O<sub>3-min</sub>) at Sheshan Island (SSI, remote and oceanic) and Xujiahui (XJH, urban) sites, respectively during 2012 to 2017.

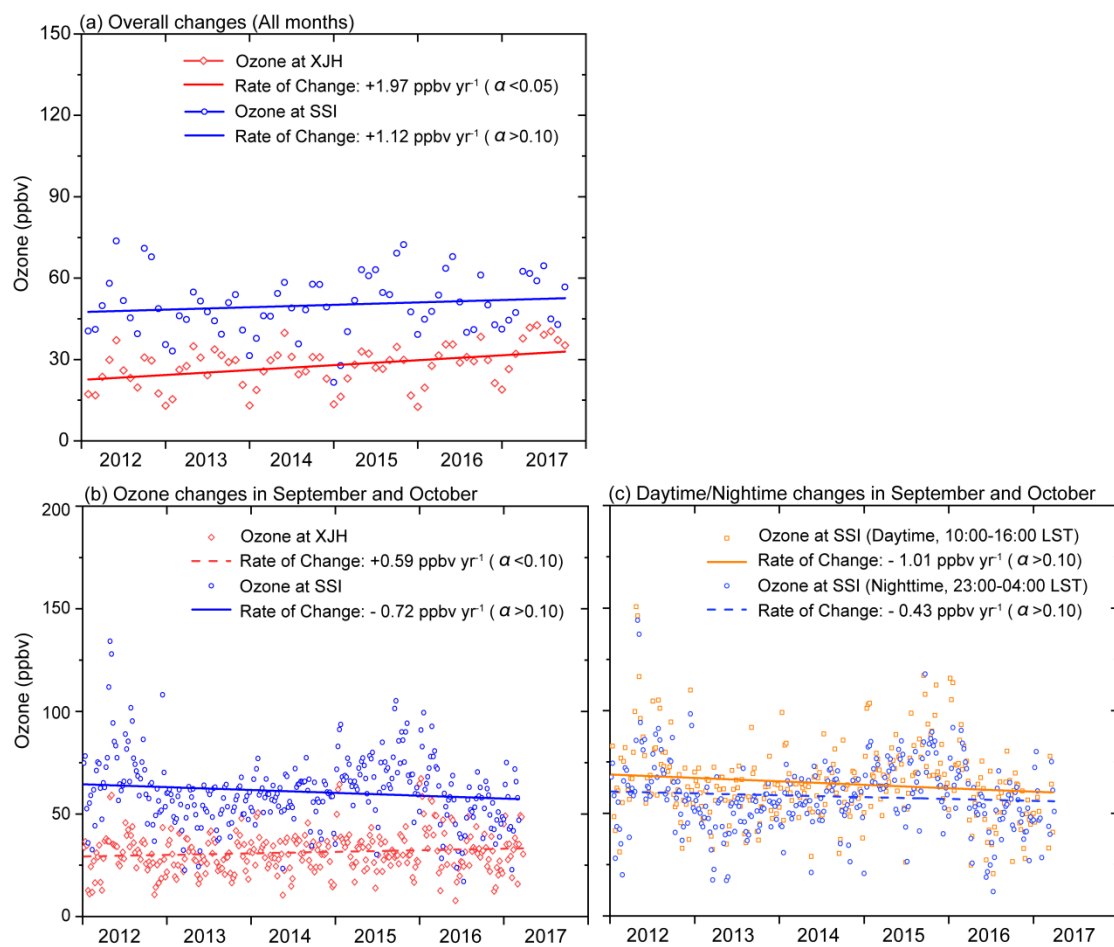


Figure 6 Variations of (a) monthly mean O<sub>3</sub> concentrations at Sheshan Island (SSI, remote and oceanic) and Xujiashui (XJH, urban) sites during the period 2012–2017, (b) corresponding variations of daily mean O<sub>3</sub> concentrations at SSI and XJH in September and October, and (c) variations of mean O<sub>3</sub> concentrations during daytime (10:00–16:00 LST) and nighttime (23:00–04:00 LST) at SSI.

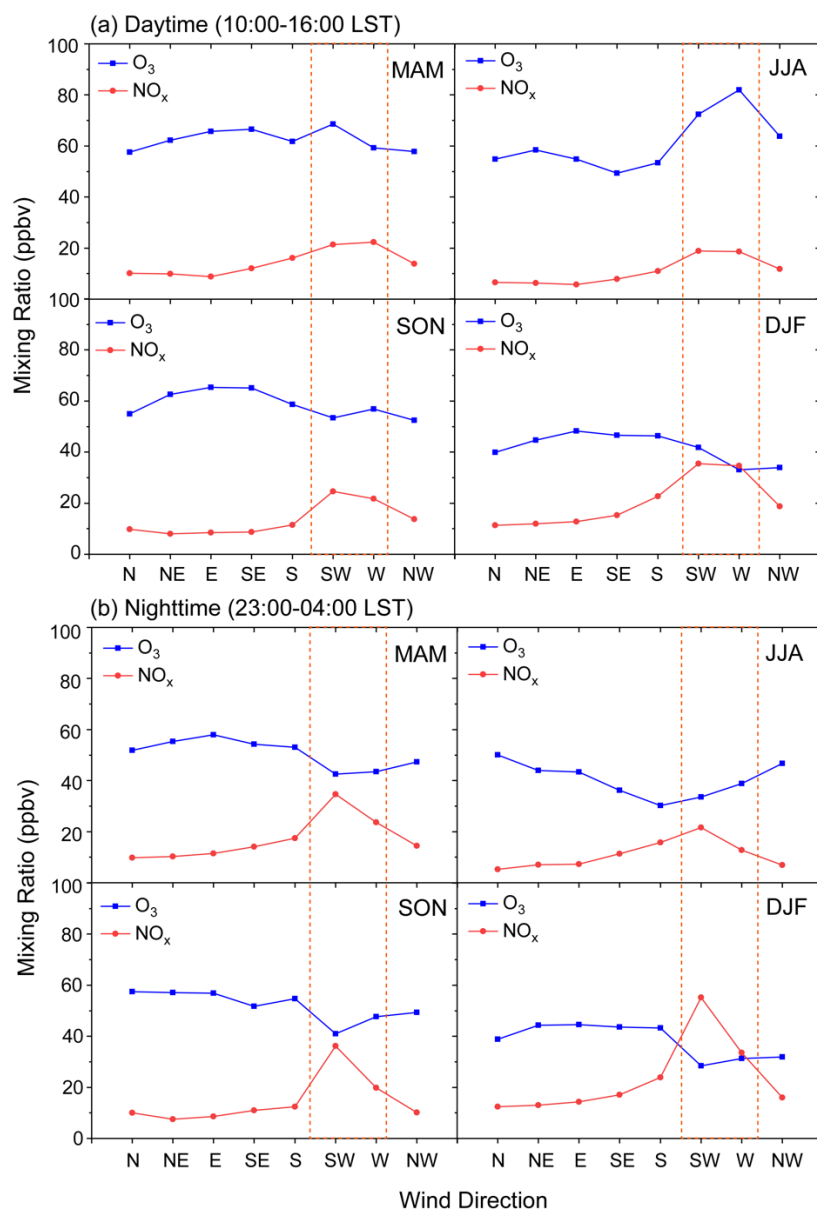


Figure 7 Daytime and nighttime mean  $O_3$  mixing ratios (ppbv) at Sheshan Island (SSI) and  $NO_x$  mixing ratios (ppbv) at Dongtan (DT) site, a remote rural site near SSI under north (N), northeast (NE), east (E), southeast (SE), south (S), southwest (SW), west (W), and northwest (NW) wind conditions in MAM (March–May), JJA (June–August), SON (September–November), and DJF (December–February), respectively during 2012 to 2017.

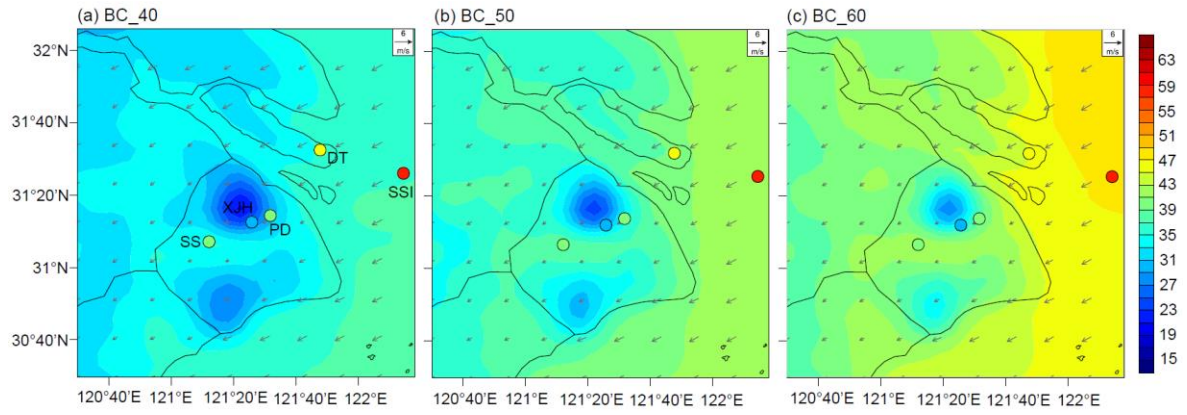


Figure 8 Calculated distributions of monthly mean  $O_3$  concentrations (shades, ppbv) from BC\_40, BC\_50 and BC\_60 simulations, respectively in September 2014. Model results are compared with observed mean  $O_3$  concentrations (circles, ppbv) obtained from Sheshan (SS), Xujiahua (XJH), Pudong (PD), DT (Dongtan) and Sheshan Island (SSI) sites. Also shown is the calculated wind field ( $m s^{-1}$ ) averaged over the same period.

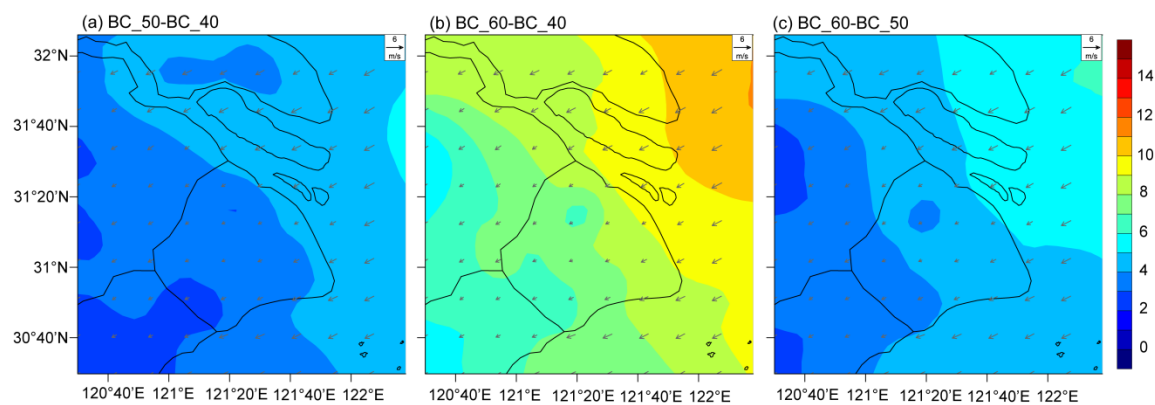


Figure 9 Mean differences in surface  $O_3$  concentrations (ppbv) simulated with different chemical boundaries: (a) BC\_50 minus BC\_40, (b) BC\_60 minus BC\_40, and (c) BC\_60 minus BC\_50 in September 2014. Also shown is the calculated wind field ( $m s^{-1}$ ) averaged over the simulation period.